CELL ADHESION TO SOLID SUBSTRATE ; ROLE OF INTERFACIAL INTERACTIONS AND RECEPTOR AGGREGATION

A thesis submitted

in partial fulfilment of the requirements

for the degree of

Master of Technology

by

SAURAV MAZUMDER

to the

DEPARTMENT OF CHEMICAL ENGINEERING

INDIAN INSTITUTE OF TECHNOLOGY, KANPUR

January, 1996

96-M-MAZ-CEL.

CERTIFICATE

Certified that the work contained in the thesis entitled "Cell adhesion to solid substrate; role of interfacial interactions and receptor aggregation", by "SAURAV MAZUMDER", has been carried out under our supervision and that this work has not been submitted elsewhere for a degree.

(Dr. Ashutosh Sharma)
Department of Chemical Engineering,
Indian Institute of Technology,
January 1996, Kanpur.

(Dr. B. S. Murthy)
Department of Civil Engineering,
Indian Institute of Technology,
January 1996, Kanpur.

Dedicated

To

My Parents

ACKNOWLEDGEMENTS

It is my privilage to convey my heartfelt thanks to my thesis supervisors, Dr. Ashutosh Sharma and Dr. B. S. Murthy. I am grateful to them for the sincere help and constructive guidance they continuously offered during this thesis work. I thank all the faculty members of the Chemical Engineering department for the support they always provided me, whenever I needed.

I wish to express my sincere thanks to my seniors, Sumeet, Khannaji, Subirda, Joydebda who were always ready to listen to my quries and forthcoming with their able suggestions, espacially Sumeet, who made it easier for me to overcome the initial difficulties in my work with his constant suggestions and encouragement. I thank my labmate Rman and all other batchmates for their warm company throughout my M.Tech curriculum. My fondest thanks go to Pavitrada and Sukanta for their encouragement and spontaneous support to solve all sort of problems I faced in my I. I. T. K days.

My words fail to acknowledge the love and support of my parents, other family members, and all my friends back home whose thoughts and worries always motivate me during my work.

ABSTRACT

The cell contact with a solid substrate is of great importance in the study of developmental biology. The interaction between a cell-membrane and a solid support can be modeled by considering the stability of the fluid film that is held in between them. This fluid film is a viscous layer which is subjected to forces like van der Waals interactions and the polar (acid-base) interactions. In the present study, two cases are considered for the stability analysis of the film, – i) effect of bending resistance offered by the cell membrane during its deformation, and ii) effect of aggregation of receptor molecules on the membrane surface. The movement of the membrane-film interface is described using a hydrodynamic approach. A systematic long-wave analysis is done to derive the nonlinear evolution equation governing the position of the said interface. For the second case, this is coupled with the evolution of the receptor concentration (based on the principle of conservation of mass). The non-linear evolution equations have been solved using appropriate numerical techniques. The results with different parameters are presented for the two cases.

Contents

List of Tables

List of Figures

NOMENCLATURE

a	space scaling parameter
a_0	area occupied by each receptor molecule
b	time scaling parameter
B	modulus of bending moment
d_0	dimensional distance of minimum separation between atoms
d	nondimensional equilibrium distance for the film
D_s	diffusion coefficient for the receptor molecules
E	nondimensional amplitude of perturbation
f	friction factor
G	free energy
h	dimensional film thickness
H	nondimensional film thickness
k	dimensional wave number of perturbation
K	nondimensional wave number of perturbation
k_c	dimensional critical wave number of perturbation
K_c	nondimensional critical wave number of perturbation
k_m	dimensional dominant wave number of perturbation
K_m	nondimensional dominant wave number of perturbation
$k_{m\gamma}$	dimensional dominant wave number considering interfacial tension only

k_{mb}	dimensional dominant wave number considering bending moment only
l_0	dimensional correlation length for the polar forces
l	nondimensional correlation length for the polar forces
M	moment produced by bending
p	film pressure
P	nondimensional ratio of polar to apolar spreading coefficients
R_1, R_2	radii of curvature
R_{λ_m}	ratio of the dominent wavelengths for the case with bending moment only to the case with interfacial tension only
S^{LW}	spreading coefficient for the apolar force
S^{AB}	spreading coefficient for the polar force
t	dimensional time
T	nondimensional time
T_l	nondimensional time of rupture obtained from linear stability analysis
x	dimensional space coordinate
X	nondimensional space coordinate

GREEK SYMBOLS

ϵ	dimensional amplitude of perturbation
γ	interfacial tension
Γ	dimensional receptor's concentration
$\overline{\Gamma}$	nondimensional receptor's concentartion
λ	dimensional wavelength of perturbation
λ_{mb}	dimensional wavelength of perturbation considering bending moment only
$\lambda_{m\gamma}$	dimensional wavelength of perturbation considering interfacial tension only
Λ	nondimensional wavelength of perturbation
μ	viscosity of the film fluid
ν	kinematic viscosity of the film fluid
ω	dimensional growth rate of the perturbation
Ω	dimensional growth rate of the perturbation
ϕ	dimensional potential due to intermoleculer interaction
Φ	nondimensional potential due to intermoleculer interaction
ρ	density of the film fluid

Chapter 1

INTRODUCTION AND LITERATURE SURVEY

In the progress of developmental biology, the determination of the developmental fate of a cell as a result of interactions with its environment has widespread applications. The environmental interaction is often caused by the specific direct influence of a solid support (extra-cellular matrix) on the cell. This type of interaction is the basic to such prosseses as histogenesis, wound healing, metastatis, neuronal organisation etc (1). Cell contacts made as a result of these processes may play important role in cell physiology. They are involved in the cell locomotion as well as in the extensive spreading and immobilization of the cell. They also contribute to the acquisition of the cell polarity, transduction of the transcellular mechanical forces, formation of the permeability barriers, control of cell growth etc (2). All of these point to the necessity of the study of the basic physics for adhesion of cells.

Several workers in the field of bio-physics have visualised this adhesion phenomenon in the light of thin film (the liquid films being thin enough so that their thermodynamics and trasport behaviours can depend on their thickness which generally ranges from 1 to 100 nm) concept of interfacial science. These two fields are combined to model the cell-support adhesion by considering the

stability of the liquid film in between the cell membrane and the support. The stability of the thin film has been analysed by employing linear theory considering only the van der Waals force as the body force (3). The nonlinear approach using long wave analysis was subsequently adopted (4). This is then further modified through incorporation of the polar forces and other specific interactions. This concept has been applied to study the cell-support interactions. The prediction of the most probable wave length for such adhesion (5), the tear film rupture analysis (6), the study of presence of receptors on the cell membrane using Marangoni effect in a non-linear approach (7) etc. can be cited as examples.

In the present work two specific characteristics of some cell-membranes are taken into consideration for the stability analysis of the film, namely the effect of resistance offered by the membrane due to the bending moments developed in it during deformation and due to interfacial tension (interfacial interactions), and the role of receptors present on the membrane surface. Bending moments are generally considered to stabilize the process of cell adhesion, providing a stabilizing effect. This effect is studied together with the interfacial tension, for different parameters of the system (like the body force term, mean film thickness etc.) to predict the actual cell-support contact or the deformed equlibrium structure in absence of cell-support contact. There are many well documented systems in which the presence of some specific molecules (lectins, SAMs, antibodies etc) is required for the cell-support adhesion to occur (8). It has been proposed that these molecules can overcome the repulsive barrier for which cell adhesion is not possible in case of bare membrane (9). It has been considered that they can form specific bonds at a short distance near the position of actual contact. In this work this phenomenon is studied in the light of effective free energy due to the presence of these receptors, for various system parameters.

Chapter 2

EFFECT OF INTERFACIAL INTERACTIONS IN CELL-SUBSTRATE ADHESION

2.1 INTRODUCTION

In the process of cell adhesion, the stabilising effect provided by the interfacial tension and the bending resistance is important. In order to account for the elastic rigidity of the membrane, the effect of bending moment has to be considered. Bending moment resists the formation of curvature on the surface (10). The effect is especially pronounced for the cases involving significant curvature changes. The present work involves the study of this influence of bending moment during the adhesion of a cell membrane on a solid support along with interfacial tension. It considers different types of cell membrane, support and the fluid film sandwitched in between them. This leads to the study of the system with different cases of the interaction potential considered to describe the body force, and varying interfacial tension.

2.2 CONCEPT OF BENDING MOMENT IN CELL MEMBRANE

Let us consider the membranes with connected bilayer (by van der Waals contact). In this case the bending moment at any point on the cell membrane and film interface can be related to the local curvature (10). If the connected bilayer is initially flat and then bent, a bending moment is produced by the effect of expansion of the upper layer and compression in the lower layer causing a small area change. This moment can be expressed as (10):

$$M = B\left(\frac{1}{R_1} + \frac{1}{R_2}\right) \tag{2.1}$$

where B is the bending rigidity constant, and is a function of the membrane properties like compressibilities of the layers and the distance between them. R_1 and R_2 are the local radii of curvature. The force due to this bending moment can be obtained as $\nabla^2 M$. Now this force is incorporated in order to balance the normal stress equilibrium condition at the cell-film interface given as follows:

$$\Delta p = -\gamma\left(\frac{1}{R_1} + \frac{1}{R_2}\right) + B\nabla^2\left(\frac{1}{R_1} + \frac{1}{R_2}\right) \tag{2.2}$$

Here $\triangle p$ is the pressure difference at any point on the membrane-film interface, and γ is the interfacial tension of that interface.

2.3 FORMULATION

A cell separated by a thin liquid film from a solid support is considered. These are separated by an interaction region which can be visualised as a non-thinning

film of thickness h , bounded laterally in the contact region with co-ordinate $x = 0$ and $x = x$. The two interfaces are at $z = 0$ (support and film interface)and $z = h$, (cell-membrane and film interface) (fig.2.1).

Starting from a reference state with a plane film of mean thickness h_0 the movement of the fluid inside the film is described by the Navier-Stokes equation for anisotropic, incompressible, non-draining and viscous fluid of viscosity μ and density ρ. The force balance is between apolar (attractive) and polar forces (attractive or repulsive). Dynamic boundary conditions are considered at the cell-film interface while the velocities are zero at the support-film interface.The boundary condition on the normal stress involves the product of the surface tension and the curvature effect, and bending moment of the cell membarane. The shear stress on the cell-film interface vanishes due to constant surface tension.

A long wave analysis (4) for this thin film (with the condition $\frac{h_0}{L} \ll 1$) leads to the evolution equation for the cell membrane ($z = h$) as follows:

$$h_t - \frac{1}{12\mu}\frac{\partial}{\partial x}[h^3\frac{\partial}{\partial x}(p + \phi)] = 0 \tag{2.3}$$

where the p and ϕ are given by (using small slope approximation):

$$p = -\gamma h_{xx} + Bh_{xxxx} \tag{2.4}$$

$$\phi = -\frac{2S^{LW}d_0^2}{h^3} - \frac{S^{AB}}{l_0}\exp(\frac{d_0 - h}{l_0}) \tag{2.5}$$

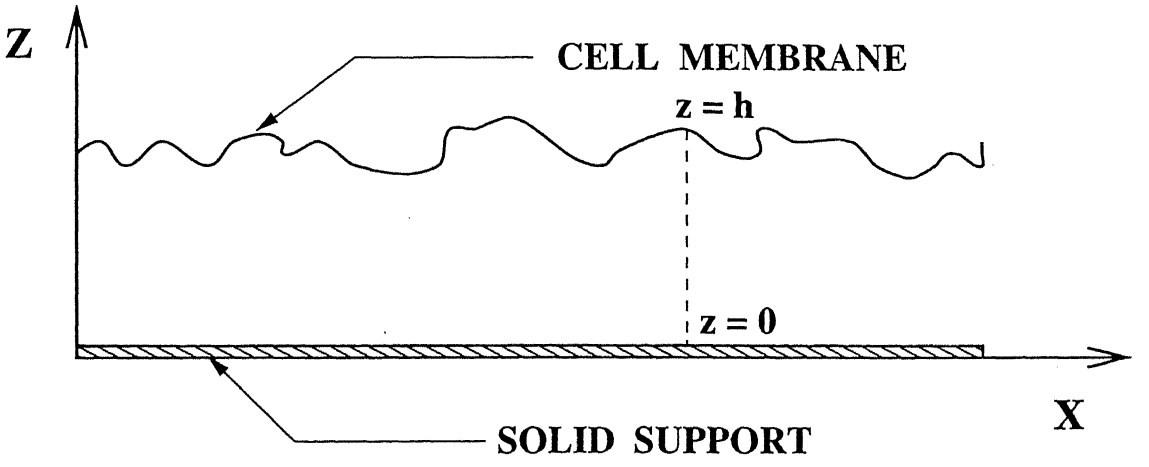

Fig. 2.1 Configuration of the system.

Here γ is interfacial tension at cell-film interface , B is bending moment of the cell membrane, S is spreading coeffcient of the film on the support in presence of the cell, LW refers to apolar and AB to polar interactions, d_0 ($\simeq 0.158$ nm) (11,12) is the equilibrium distance for the film where the born repulsion may be replaced by a vertical rise in the potential to infinity (hard sphere approximation) and l_0 ($\simeq 0.6$ nm) (11,12) is the correlation length for the polar forces.

NON-DIMENSIONALISATION:

The above equations can be non-dimensionalised using the following non-dimensional parameters to retain mininmum number of parameters and for compact representation:

$$H = \frac{h}{h_0}, d = \frac{d_0}{h_0}, l = \frac{l_0}{h_0},$$
$$P = -\frac{S^{AB}}{S^{LW}(6d^2l^2)},$$

and non-dimensional space and time scalings,

$$X = \frac{ax}{h_0}, T = \frac{bt\nu}{h_0^2}, \tag{2.6}$$

where

$$a = \left(\frac{6\left|S^{LW}\right| d^2 h_0^2}{B}\right)^{\frac{1}{4}}, \; b = \frac{d^2 h_0 \left|S^{LW}\right| a^2}{2\nu^2\rho}, \; \nu = \frac{\mu}{\rho}. \tag{2.7}$$

Now the evolution equation can be written in a form that involves least number of parameters, namely, P, d, l and A which solely depend on surface properties ($\gamma, B, S^{LW}, S^{AB}$) and the mean film thickness h_0 :

$$H_T = \left[H^3 \left(-AH_{XXX} + H_{XXXXX} \right) + sgn\left(S^{LW} \right) \left(H^{-1} - P \exp\left(\frac{d-H}{l} \right) H^3 \right) H_X \right]_X \tag{2.8}$$

where the function $sgn(S^{LW})$ refers to the sign of S^{LW} i.e, $sgn(S^{LW}) = +1$ if $S^{LW} > 0$, and for $S^{LW} < 0$ it is -1 and A is given by:

$$A = \frac{\gamma h_0}{\left(6 \left| S^{LW} \right| B d^2\right)^{\frac{1}{2}}}. \tag{2.9}$$

The second and third term of the equation [2.8] are related to the stabilizing influence of the film interfacial tension and bending moment respectively. The remaining non-linear terms which account for the excess free energy (ϕ) of the film, may be stabilizing or destabilizing, depending on the signs of S^{LW} and S^{AB}. When S^{LW} is negative Lifshitz-van der Waals forces are destabilizing and vice-versa. The same applies for the polar interactions based on the sign of S^{AB}. The dynamics of the film is therefore dictated by the balance of nonlinear effect of the film tension and bending moment and the apolar and polar intermoleculer forces. The role of the non-dimensional parameter A is in studying the effect of the interfacial tension together with the effect of bending moment.

2.4 LINEAR STABILITY ANALYSIS

The initial (short time) evolution of the film profile is adequately described by linearized equation whenever the amplitude of the initial disturbance is much smaller than the mean film thickness. In order to get an initial estimate of the behaviour and the associate time scale of the film for infinitesimal perturbations,

linearization around the mean film thickness can be done. For the linear evolution equation [2.3] this mean film thickness can be taken at $h = h_0$ and for the nondimensional [2.8] one this will be $H = 1$, are done. Linearization leads to the following solutions respectively:

$$h = h_0 + \epsilon \sin kx \exp(\omega t) \tag{2.10}$$

$$H = 1 + E \sin KX \exp(\Omega T) \tag{2.11}$$

where ϵ is the dimensional amplitude ($\epsilon \ll h_0$) and E is defined as the ratio of ϵ to h_0. The dimensional growth coefficient ω is related to the dimensional wave number, k as (4):

$$\omega = \frac{1}{3\mu}\left[-h_0^3\left(\gamma k^4 + Bk^6\right) - h_0^3 k^2 \left(\phi_h\right)_{h_0}\right] \tag{2.12}$$

where $\left(\phi_h\right)_{h_0}$ refers to the derivative of ϕ with respect to h, evaluated at h_0.

Similarly the non-dimensional growth coefficient Ω can be expressed by the following equation:

$$\Omega = -AK^4 - K^6 - sgn\left(S^{LW}\right)\left[1 - P\exp\left(\frac{d-1}{l}\right)\right]K^2 \tag{2.13}$$

where K is the nondimensional wave number.

Now the critical wave number k_c ($0 < k < k_c$) is defined for $\omega = 0$, since the surface instability can only grow if $\omega > 0$:

$$k_c = \sqrt{\frac{-\gamma + \sqrt{\gamma^2 - 4B\left(\phi_h\right)_{h_0}}}{2B}} \tag{2.14}$$

According to the linear theory, the fastest growing initial disturbance has a wave number k_m (known as dominant wave number), obtained from the solution of $\frac{\partial \omega}{\partial k} = 0$,which gives:

$$k_m = \sqrt{\frac{-\gamma + \sqrt{\gamma^2 - 3B\left(\phi_h\right)_{h_0}}}{3B}} \tag{2.15}$$

Two asymptotic cases can be derived from the above equation, as shown below:

For $B \rightarrow 0$

$$k_{mB} = \sqrt{\frac{-\left(\phi_h\right)_{h_0}}{2\gamma}} \tag{2.16}$$

and $\gamma \rightarrow 0$

$$k_{m\gamma} = \left(\frac{-\left(\phi_h\right)_{h_0}}{3B}\right)^{\frac{1}{4}} \tag{2.17}$$

Similarly the expressions for the nondimensional critical and dominant wave numbers can be found from the following equations respectively:

$$K_c = \sqrt{\frac{-A + \sqrt{A^2 - 4sgn\left(S^{LW}\right)\left(1 - P\exp\left(\frac{d-1}{l}\right)\right)}}{2}} \tag{2.18}$$

$$K_m = \sqrt{\frac{-A + \sqrt{A^2 - 3sgn\left(S^{LW}\right)\left(1 - P\exp\left(\frac{d-1}{l}\right)\right)}}{3}} \tag{2.19}$$

Thus the non-dimensional wave length (in X coordinate) for the dominant mode of disturbance is given by $\Lambda_m = \frac{2\pi}{K_m}$ and its rate of growth (in T coordinate) is given by [2.13] ,replacing K by K_m. The dimensional case can be treated in a similar way.

From linear theory one can predict a hypothetical time of rupture (nondimensional) by setting $H = 0$ at $\sin(KX) = -1$. This gives a linear estimate for the time of film rupture T_L, for a perturbation of wave number K , given by:

$$T_L = \left[\frac{1}{\Omega K}\right] \ln\left(\frac{1}{E}\right) \tag{2.20}$$

The dimensional case can be treated in the similar way for evaluating dominant wave length and the linear time of rupture.

2.5 NONLINEAR ANALYSIS

Since the linear theory underestimates the nonlinear terms in the evolution equation at the cell-film interface, it fails to predict either qualitatively or quantitavely the ultimate fate of the system. This necessitates the nonlinear analysis of the system. Here to understand the effect of the bending moment of the cell membrane on the evolution equation, the entire study is done in two parts, namely,

1. The cases with no polar interactions ($P = 0$)

2. The cases with polar interactions.($P \neq 0$)

For all of the above cases the effect of interfacial tension is observed by varying the values of γ at constant h_0, and the effect of mean film thickness is studied by the reverse way. The value of A is also varied as a lumped parameter for some cases.

NUMERICAL METHOD:

The sixth order nonlinear equation [2.8] may be solved with periodic boundary conditions over a wavelength, $\Lambda = \frac{2\pi}{K}$,viz.,

$$\left(\frac{\partial^i H}{\partial X^i}\right)_{X=0} = \left(\frac{\partial^i H}{\partial X^i}\right)_{X=\lambda}, (i = 0, 1, ..., 5); 0 \leq X \leq \lambda \tag{2.21}$$

and a periodic initial condition can be used on the basis of initial perturbation as:

$$H(0, X) = 1 + E \cos KX, (|E| < 1) \tag{2.22}$$

Cosine perturbation is taken as initial condition due to its symmetric nature about the mid-plane of the wavelength. This even reduces the computational time, since in this case the actual simulation for half the wavelength is sufficient, the other half being the mirror image of that. Fourier collocation technique (13-15) is used for discretization. The number of grid points required for accuracy is around 50 in the half wavelength. It is the most straight forward method for the problem with spatial periodicity. An automatic adjustment of the time step was employed by using the Gear algorithm for time integration. This becomes increasingly important near the time of rupture (16). The periodicity interval is first normalized to $(0, 2\pi)$ by rescaling the X coordinate as:

$$\eta = KX, \ 0 \leq \eta \leq 2\pi \tag{2.23}$$

The discretization of the evolution equation and initial and boundary conditions are done in the following way (17). Eq.[2.8], rewritten in η coordinate, is then exactly satisfied at N (even integer) number of Fourier collocation grid points (the end point is omitted due to periodicity).

$$\eta_j = 2\pi\,(j-1)\,/N,\ j = 1, 2, ..., N. \tag{2.24}$$

The collocation points are related to the discrete Fourier coefficients of the film thickness, a_k

$$a_k = (1/N)\sum_{j=1}^{N} H\,(\eta_j)\exp^{-ik\eta_j},\ -(N+1)\,/2 \leq K \leq (N+1)\,/2 \tag{2.25}$$

In view of this, Fourier collocation differentiation can be represented by a $N \times N$ skew-symmetric matrix, $\mathbf{D}_N$ with components

$$\begin{aligned}(\mathbf{D}_N)_{ij} &= (1/2)\,(-1)^{i+j}\cot\left[(i-j)\,\pi/N\right],\ i \neq j \\ &= 0,\ i = j\end{aligned} \tag{2.26}$$

The higher order derivative matrices, $\mathbf{D}_N^2$, $\mathbf{D}_N^3$ and $\mathbf{D}_N^5$, etc. are simply obtained by n multiplications of the matrix $\mathbf{D}_N$, where n equals the order of derivative.

The requirement that eq. [2.8] is exactly satisfied at each of the collocation points, gives a set of N equations.

$$\begin{aligned}\frac{\partial \mathbf{H}}{\partial T} + AK^4\left[\mathbf{D}_N\left\{\mathbf{H}_3\left(\mathbf{D}_N^3\mathbf{H}\right)\right\}\right] + K^6\left[\mathbf{D}_N\left\{\mathbf{H}_3\left(\mathbf{D}_N^5\mathbf{H}\right)\right\}\right] \\ -sgn(S^{LW})K^2\mathbf{D}_N\left[\Phi_{\mathbf{H}}\mathbf{H}_3\left(\mathbf{D}_N\mathbf{H}\right)\right] = 0\end{aligned} \tag{2.27}$$

where $\mathbf{H}$ is a column vector of film thickness,

$$\mathbf{H} = (H(\eta_1, T),\ H(\eta_2, T), ..., H(\eta_N, T)). \tag{2.28}$$

$\mathbf{H_3}$ is a $N \times N$ diagonal matrix with jth diagonal element equal to $H_j^3(\eta_j, T)$, and $\Phi_{\mathbf{H}}$ is $N \times N$ diagonal matrix with kth diagonal element equal to

$$\Phi_{kk} = \left[H_k^{-4} - P \exp\left\{(d - H_k)/l\right\}\right], \tag{2.29}$$

The N initial conditions are written as:

$$\mathbf{H}_i(\eta_i, 0) = 1 + E\cos(\eta_i),\ i = 1, 2, ..., N \tag{2.30}$$

The time integration is done using the package D02EJF from NAG library and it is continued until the film goes to rupture (when at some localized point the minimum film thickness is falling below the cut-off thickness, d_0) or assumes some time independent profile.

2.6 RESULTS AND DISCUSSION

Based on the parameter values (11,12,18) of tables (2.1) and (2.2), the spreading coefficients S^{LW} and S^{AB} are calculated for different cases from the following equations, using the concept given in the appendix of (17):

$$S^{LW} = 2\left[\sqrt{\gamma_c^{LW}} - \sqrt{\gamma_f^{LW}}\right]\left[\sqrt{\gamma_f^{LW}} - \sqrt{\gamma_s^{LW}}\right] \tag{2.31}$$

$$S^{AB} = 2\left[\begin{array}{c}\sqrt{\gamma_f^+}\left(\sqrt{\gamma_c^-} + \sqrt{\gamma_s^-} - \sqrt{\gamma_f^-}\right) + \sqrt{\gamma_f^-}\left(\sqrt{\gamma_c^+} + \sqrt{\gamma_s^+} - \sqrt{\gamma_f^+}\right) \\ -\sqrt{\gamma_c^-\gamma_s^+} - \sqrt{\gamma_c^+\gamma_s^-}\end{array}\right] \tag{2.32}$$

Table 2.1: Different components of γ in mJ/m^2 for different cells and water

	γ^{LW}	γ^+	γ^-
Erethrocytes	35.2	0.01	46.2
Lymphocytes	27.7	0	32.2
Corneal epithelial	27.4	3.2	56.3
water	21.8	25.5	25.5

Table 2.2: Different components of γ in mJ/m^2 for different substrates

	γ^{LW}	γ^+	γ^-
Agarose	41	0	34
Polystyrene	42	0	1
Cellulose acetate	38	0	33
teflon	17	0	0

where the suffixes c, f, and s denote cell, film, and support respectively. LW and AB refer to the apolar and polar components respectively. The typical value of the bending modulus B can be taken as 10^{-13} ergs (7) for all the cases described below.

The relative importance of bending moment and interfacial tension will be clear if the dominant wavelengths for these two cases are compared. The value of dominant wavelength $\left(\lambda_{mB} = \frac{2\pi}{k_{mB}}\right)$, for the case with bending moment and no interfacial tension, is obtained by using eq. [2.17].

$$\lambda_{mB} = 2\pi \left(\frac{3B}{(-\phi_h)_{h_0}}\right)^{\frac{1}{4}} \tag{2.33}$$

Similarly, for the case with interfacial tension and no bending moment the dominant wavelength can be written as [2.16]:

$$\lambda_{m\gamma} = 2\pi \left(\frac{2\gamma}{(-\phi_h)_{h_0}}\right)^{\frac{1}{2}} \tag{2.34}$$

The ratio (R_{λ_m}) for these two dominant wavelengths, corresponding to the above two cases is given as:

$$R_{\lambda_m} = \frac{\lambda_{mB}}{\lambda_{m\gamma}} = \left(\frac{3B\,(-\phi_h)_{h_0}}{4\gamma^2}\right)^{\frac{1}{4}} \tag{2.35}$$

This can be expressed in terms of nondimensional quantities:

$$R_{\lambda_m} = \frac{P_0}{\sqrt{A}} \tag{2.36}$$

where:

$$P_0 = \left[-\frac{3}{4} sgn\left(S^{LW}\right)\left(1 - P\exp\left(\frac{d-1}{l}\right)\right)\right]^{\frac{1}{4}} \tag{2.37}$$

and A is given by eq. [2.9].

For different sets of values of γ and h_0 (at constant B), the values of $\lambda_{m\gamma}$ are listed in table (2.3). Typical values of S^{LW} and S^{AB} are taken to be the same as those for a system with water film separated by polar cell-membrane and apolar solid support. It is clear from the table that for low values of γ, the effect of bending moment has to be included in the stability analysis of the film. Otherwise the length scale of instability would be much lower than the typical dimensions of the cells (0.01 to 1 μm). Also the theory of long wave analysis is not found to be valid for these cases, since the wavelengths are smaller than the mean film thickness. However, h_0 remaining constant, the values of λ_{mB} are of the same order as the cell dimensions (shown in table 2.4). Long wave analysis is also seen to be applicable in this case. On the other hand, for higher values of γ with high h_0, the effect of bending moment may be neglected. The variation of R_{λ_m} with typical values of A and P_0 is shown in fig.(2.2). The low values of A and high values of P_0, characterised by low γ and h_0, correspond to the high values of R_{λ_m}.

Now we can broadly classify the study into two parts. This is based on the type(s) of potential selected to describe the free energy of the system.

2.6.1 CASE : 1 $P = 0$.

In this case only apolar interactions are taken into account. This is the case when the film fluid and either the cell membrane or the support are apolar, i.e. both the polar components (γ^+ and γ^-) for them are zero (e.g. hydrocarbon films in contact with lymphocyte cell). S^{LW} has to be negative in this case to describe the attractive behaviour of the van der Waals force.

Table 2.3: Values of $\lambda_{m\gamma}$ for different γ at different h_0, $S^{LW} = 2mJ/m^2$ and $S^{AB} = -33mJ/m^2$.

γ (mJ/m^2)	h_0 (nm)	$\lambda_{m\gamma}$ (μm)
0.001	2	0.00013
0.001	8	0.0256
0.1	2	0.0013
0.1	8	0.2
1	2	0.0043
1	8	0.8113

Table 2.4: Values of λ_{mB} for different for different h_0, $S^{LW} = 2mJ/m^2$ and $S^{AB} = -33mJ/m^2$.

h_0 (nm)	2	4	6	8
λ_{mB} (μm)	0.0102	0.0236	0.0547	0.1382

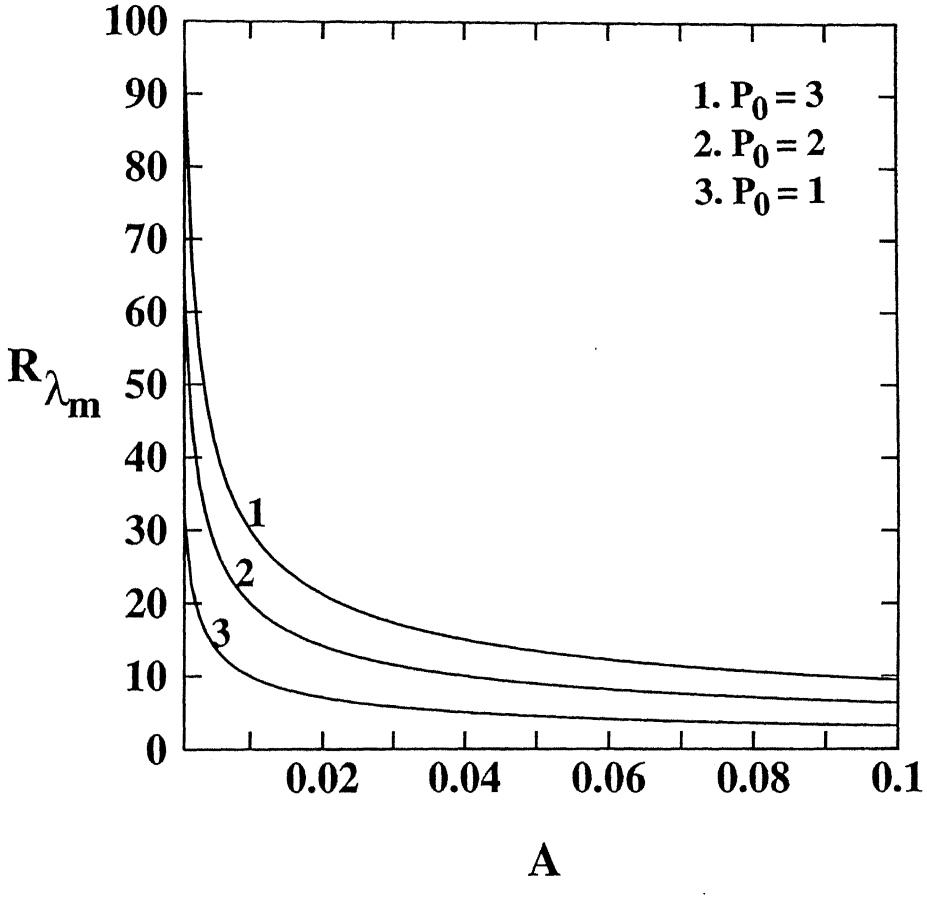

Fig. 2.2 Variation of R_{λ_m} with A for diiferent P_0.

For this case the linear theory predicts the inverse dependence of the dominant wave number with γ and h_0 and hence with A (from equation (2.19) making $P = 0$). This shows the direct variation of dominant wavelength with these quantities. From nonlinear analysis it is found that bending moment can never overcome the destabilizing effect of LW force, so eventually rupture occurs in all cases. This implies that actual cell-support contact is possible for these cases. From fig.(2.3) it is clear that the time of rupture (T_R) is minimum for a given A at some specific wavelength , which corresponds to $K = K_m$. T_R increases with A (fig.2.3) for the dominant wave ($K = K_m$) as well as for the other wave numbers. This is due to the decrease of K_m with increasing A (from linear theory) which again retards the growth rate of perturbation. Increase of A signifies an increase in the interfacial tension at constant mean film thickness (unlike h_0, γ has no contribution to the scaling parameter b for time), which makes the system more stable.The profiles at the time of rupture are shown in fig.(2.4) for different A at K_m. The difference in the profiles is primarily due to the difference in K_m which leads to different length scales of instability. The effect of different length scales of perturbation on the rupture profile for a given A, is shown in fig.(2.5) .

2.6.2 CASE : 2 ($P \neq 0$).

This is the case when both polar and apolar interactions are taken into account to evaluate the free energy. For all of the following cases, the cell-membrane is taken to be polar in nature (e.g. erethrocytes etc). According to the nature of the solid support this analysis is divided into two parts. For the first part the substrate (the solid support) is apolar (e.g. teflon). So the polar interactions arise solely due to the polarity of the film-fluid and the cell-membrane. Typical

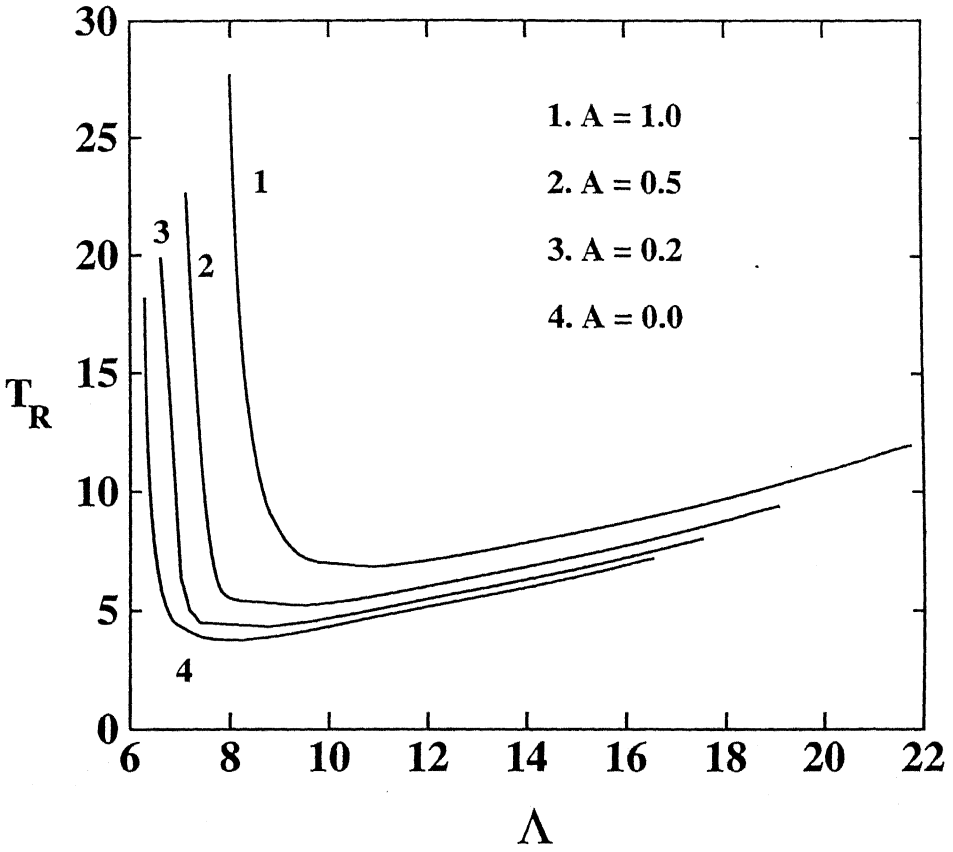

Fig. 2.3 Variation of time of rupture with wavelength in nondimensional form for different A. Apolar case.

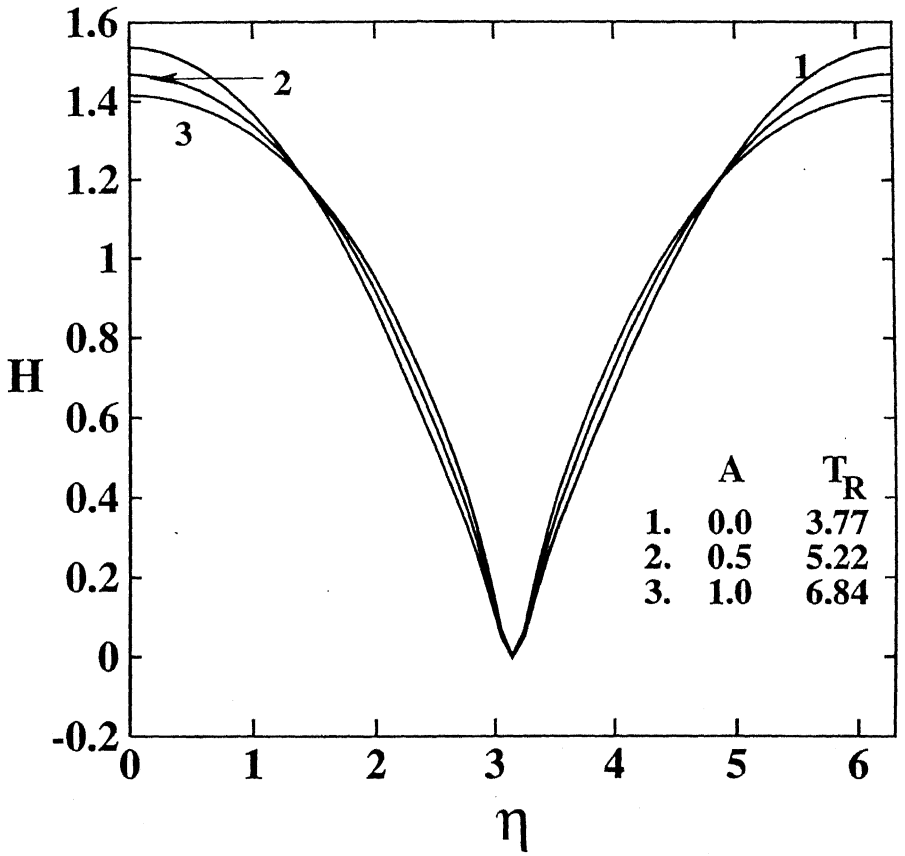

Fig. 2.4 Nondimensional profiles at the time of rupture for different A. Apolar case. The values of dominant wavelengths for the three curves are 8.26, 9.53 and 10.88 respectively.

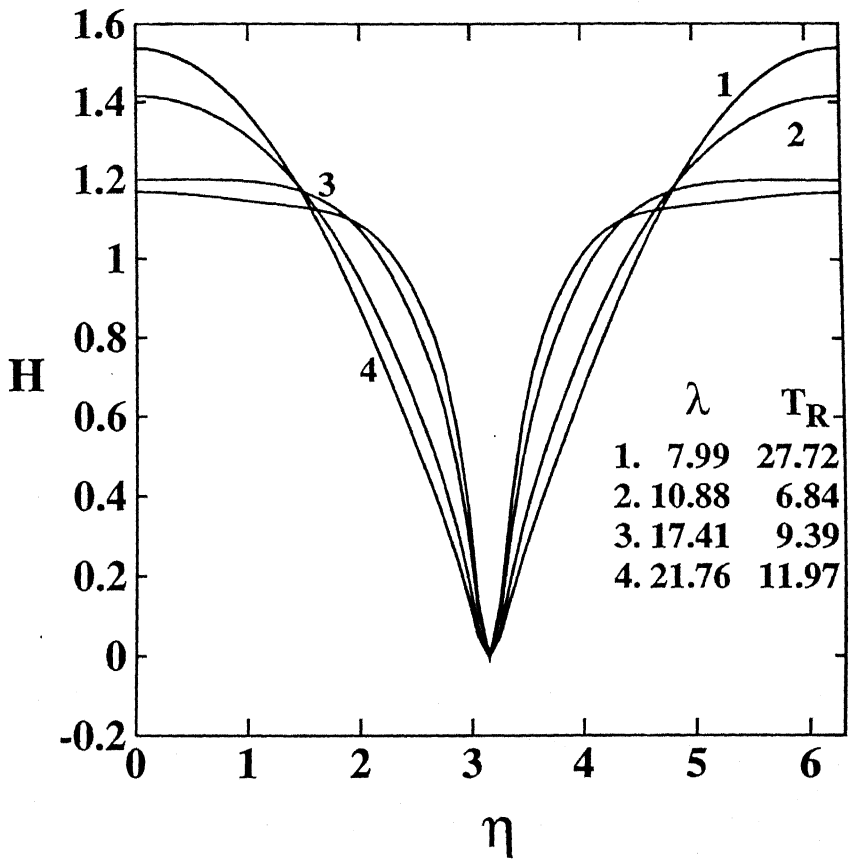

Fig. 2.5 Nondimensional profiles at the time of rupture for different wavelength. A=1. Apolar case.

values of the components of the interfacial tension are taken such that $S^{LW} > 0$ ($\gamma_c^{LW} > \gamma_f^{LW} > \gamma_s^{LW}$), and $S^{AB} < 0$ ($\gamma_s^- > \gamma_c^-/4$) (17). This leads to the system where AB interaction is destabilizing and LW interaction is stabilizing. For the next part the substrate is polar, thus at least one of the polar components of the interfacial tension is non-zero (e.g. agarose,cellulose acetate etc). In this case $S^{LW} < 0$ (destabilizing effect) and $S^{AB} > 0$ (stabilizing effect). As in the previous case the conditions for the different components of the interfacial tensions of the three members of the system are chosen according to the relations given in the appendix in (17). Here the first case resembles the region 4 and the second one, region 2 of the fig.2 in (17). For the apolar support, the values of the spreading coefficients are: $S^{LW} = 2$ mJ/m^2, and $S^{AB} = -33$ mJ/m^2 and those for the polar support are taken to be: $S^{LW} = -4$ mJ/m^2, and $S^{AB} = 25$ mJ/m^2 . The properties of the fluid film is taken to be the same as those of water.

The variation of the second derivative of the total free energy (ϕ_h) with respect to the film thickness is shown in fig.(2.6). It is evident from the two curves that ϕ_h is positive for the apolar case (fig.2.6a) beyond the film thickness 8.8 nm, whereas that for the polar case is below 8.1 nm (fig.2.6b). So these two curves are similar to the part in between h_1 and h_2 of the region 4 and region 2 of the fig.2 in (17), respectively. For both these cases a critical value of $h = h_c$ can be defined beyond which the competition between the two components of the free energy is more pronounced (17). The values of h_c are estimated here at those points where the simulation results with the Fourier collocation technique show rupture (17) (though in the actual case there is indeed significant competition between the stabilizing and the destabilizing term(s), but no rupture is observed employing a efficient finite difference approach for discretization, which will be discussed in the next chapter). The results are obtained for the analysis in the

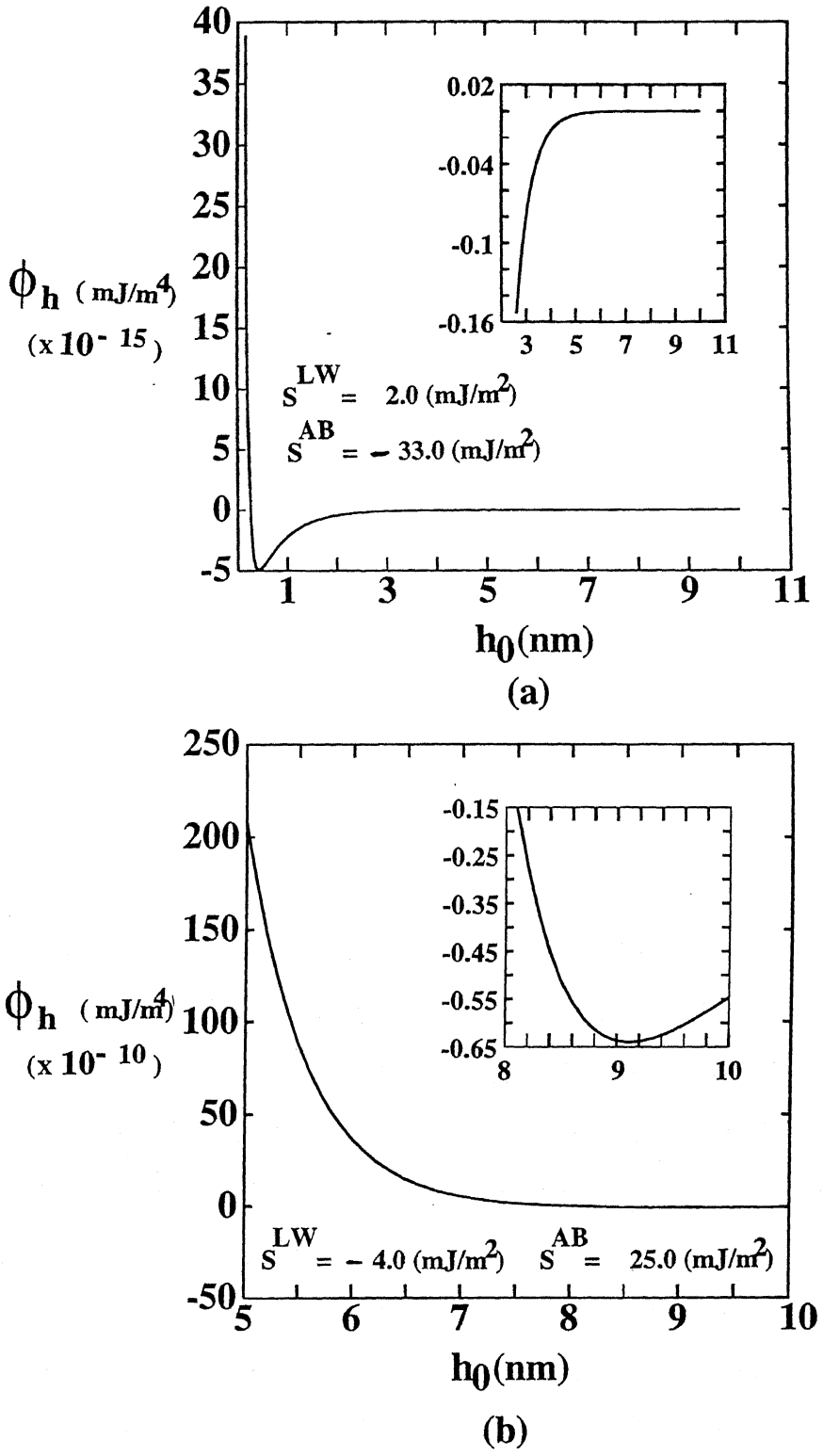

Fig. 2.6 Variation of ϕ_h with mean film thickness.
Curve (a) for apolar support and (b) for polar support.

Following two cases with h_0 near or beyond the h_c, as these cases are expected to be more interesting to study the additional effect of bending moment.

The results from the linear stability study are shown in fig.(2.7). It deals with the variation of the critical wavelength Λ_c at $K = K_c$ with the mean film thickness within the limit $\phi_h < 0$. For both these cases it is clear from the figure that the value of Λ_c is much greater than the value of h_0 at any specific point on the curves, satisfying the criterion for long wave analysis which is given as $\Lambda_c / h_0 > 1$. It is also obvious from this discussion that this criterion will be automatically satisfied for the apolar case, since in that case the K_c values will be smaller since $P = 0$ [2.18]. The general qualitative result from the nonlinear study is that in this case the actual cell-support contact never takes place. This finding is elaborated in the following subsections.

- APOLAR SUBSTRATE:

Fig.(2.8) shows the profiles at the time of rupture for different starting mean film thickness at constant interfacial tension. The apparent difference in the peak values of the profiles for different h_0 is again due to the difference in the length of the unit cell in which the instability evolves, owing to the decreasing K_m for the different cases, with increasing h_0. But the nondimensional time of equilibriation increases with increasing h_0 as shown in the figure (and hence the the dimensional time , $t \propto T h_0$; [2.6]). This is because at higher h_0 the increase in the magnitude of P ($\propto h_0^4$) is much greater than that of A ($\propto h_0^2$), thereby causing more destabilization. Fig.(2.9) shows the effect of γ at constant h_0. Here again the difference in the peak values can be physically resolved as earlier. The nondimensional time decreases with increasing γ (also the dimensional time, $t \propto T$ [2.6]) as in the figure. This can be attributed to the stabilizing nature of

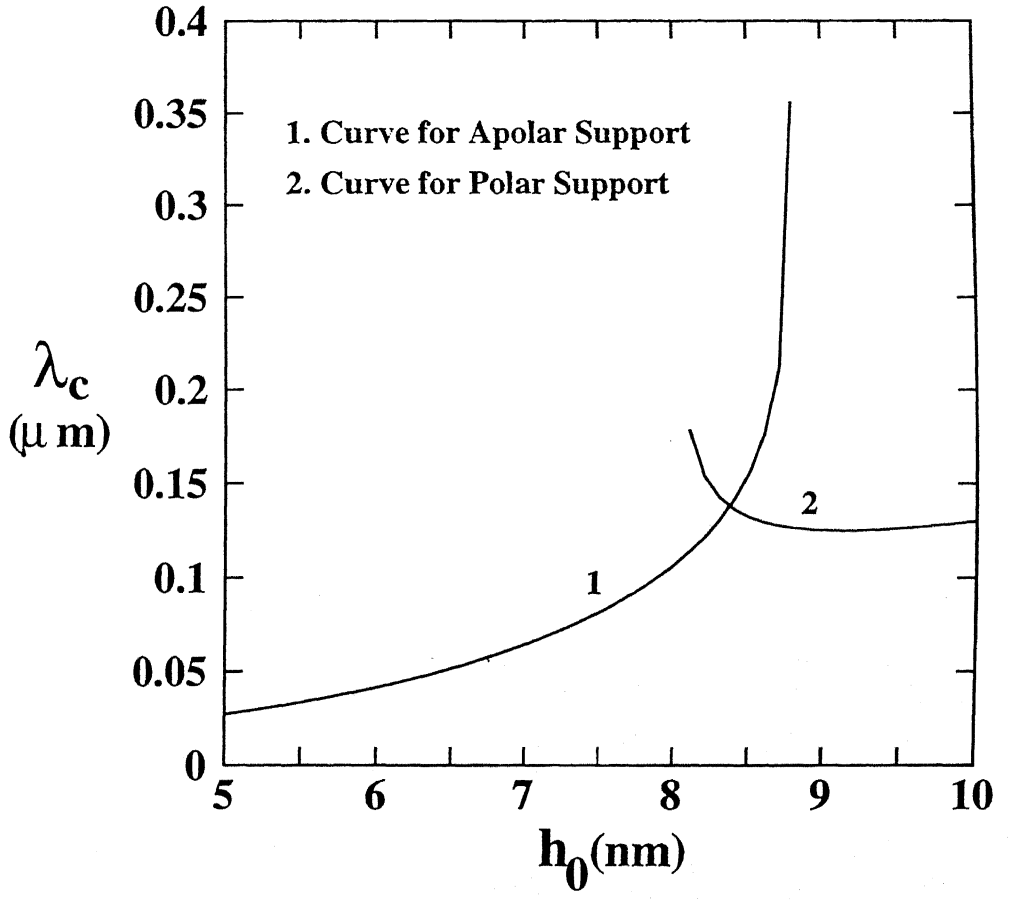

Fig. 2.7 Variation of critical wavelength with mean film thickness. $\gamma = 0$. The values of the spreading coefficients for the curves 1 and 2 are same as those in fig. 1.6. Polar case.

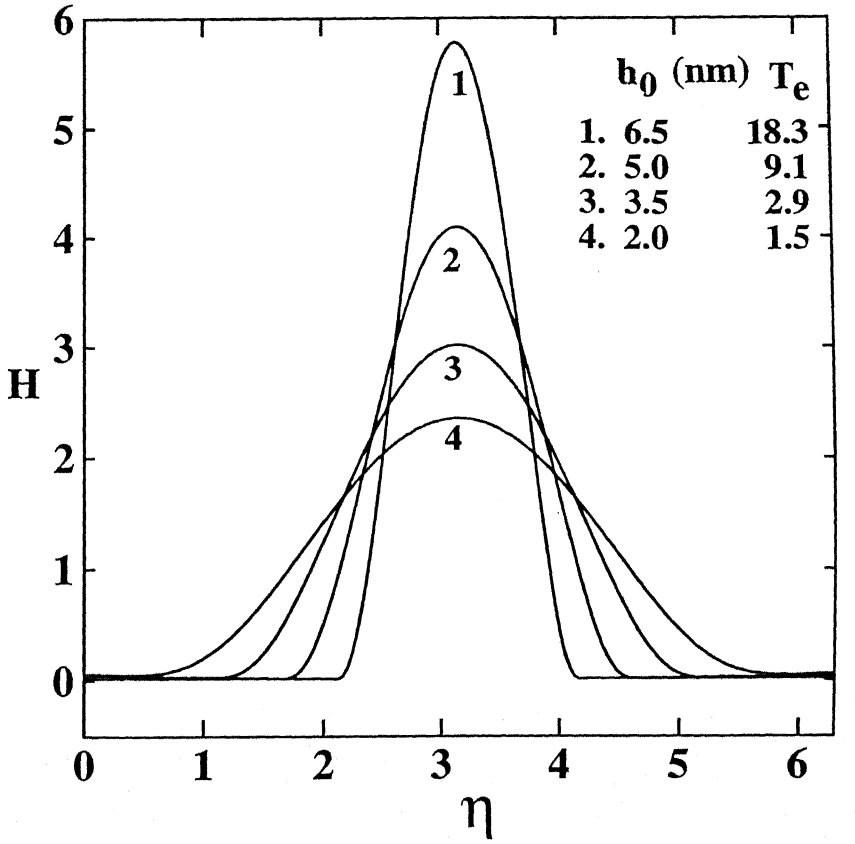

Fig. 2.8 Nondimensional equilibrium profiles of the film for different mean film thickness. Polar case with apolar support. $\gamma = 0.001 mJ/m^2$, $S^{LW} = 2 mJ/m^2$ and $S^{AB} = -33 mJ/m^2$. The values of A, minimum nondimensional thickness at equilibrium and nondimensional dominant wavelengths for the four curves are given respectivaly as - Curve 1: 0.0244, 0.0199, 4.36 ; Curve 2: 0.0144, 0.0246, 2.98 ; Curve 3: 0.007, 0.0346, 2.27 ; Curve 4: 0.0023, 0.0587, 2.132.

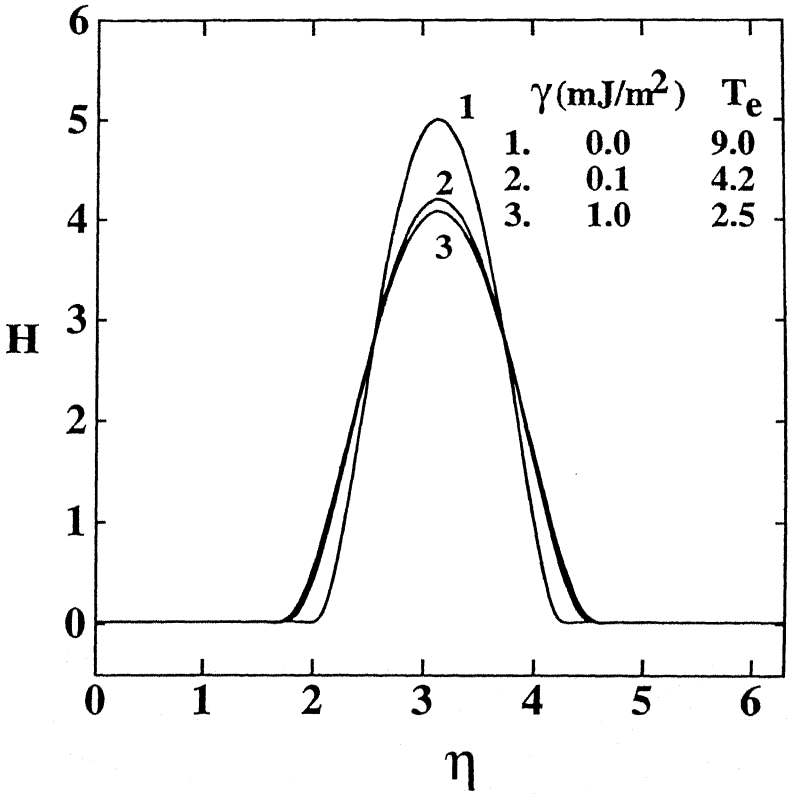

Fig. 2.9 Nondimensional equilibrium profiles of the film for different values of interfacial tension. Polar case with apolar support. Mean film thickness = 5 nm. The spreading coefficients are same as in fig. 1.8. The values of A, minimum nondimensional thickness at equilibrium and nondimensional dominant wavelengths for the three curves are given as - Curve 1: 0.0, 0.019, 2.986 ; Curve 2: 1.44, 0.020, 3.15 ; Curve 3: 14.44, 0.023, 4.78.

interfacial tension. However for both the above cases the dimensional time of equilibriation is in the order of micro- to milli- seconds which signifies the spontaneous attainment of equilibrium. Again the nondimensional time of equilibriation for all of the above cases has the maximum order of 10 and the difference in the equilibiation time for the various cases is not significant and will not be observed in reality. So physically the stabilizing effect of the bending moment will not be that apparent.

A specific study for the evolution of the cell-film interface with time for a typical case of $\gamma = 0.001$ mJ/m^2 and $h_0 = 5$ nm at $K = K_m$ is shown in fig.(2.10). It can be easily inferred from the figure that initially two drops are formed from the original perturbation which then coalesce to give one drop. Afterwards this drop starts thinning due to the destabilizing forces. Ultimately the stabilized equilibrium profile is attained (as evident from the fact that there is no change in it even after the lapse of long time) when the stabilizing components overcome the destabilizing ones. It is interesting to note that the time taken for the formation of the two drops from the original perturbation is much greater than that for equilibriation from the two drops. This is because at higher film thickness the body forces are insignificant in comparison to the interfacial tension which has slow effect on the process of evolution . But as soon as the small film thickness (at least at some points) is attained the body force terms become dominating, therefore dictate the ultimate fate of the film immediately.

Among the six profiles shown in this figure, curves 1,2,4 and 6 are used to estimate the evolution of the complex nanostructures in three dimension, as given by the contour plots of fig.(2.11). These structures are a combination of the holes, films, islands, and rims as anticipated in (19). Such structures are witnessed in reality in the stability of thin films for different systems (20,21).

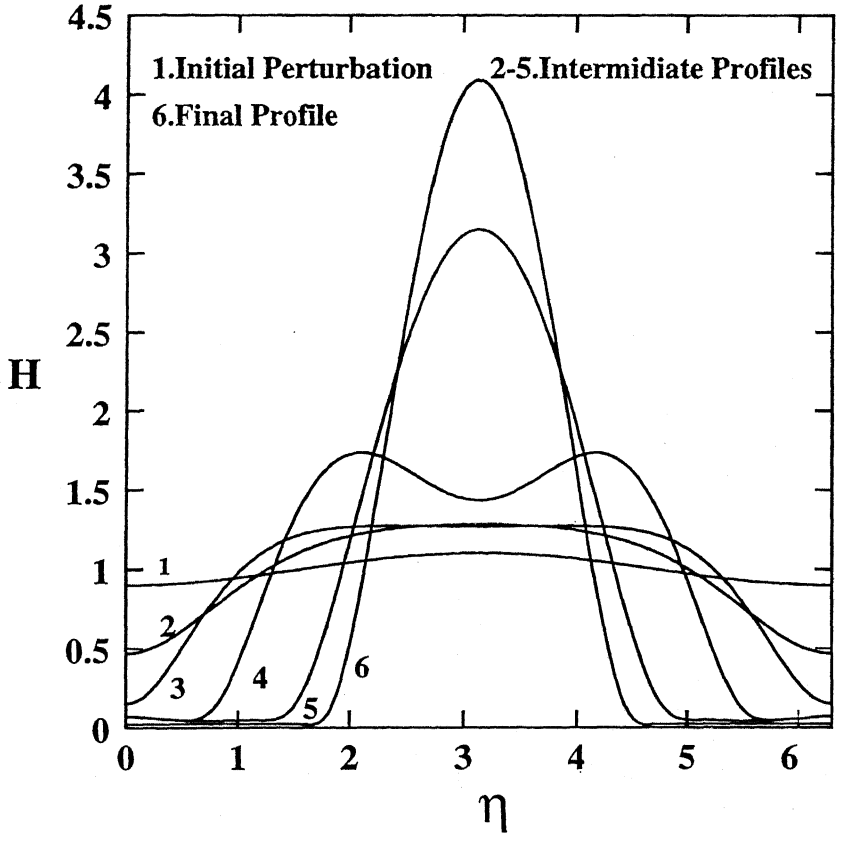

Fig. 2.10 Evolution of film profile with time. Mean film thickness = 5 nm. Interfacial tension = 0.001 mJ/m^2. Spreading coefficients are same as in fig. 1.8. A = 0.0144. The nondimensional dominant wavelength = 2.98. Minimum nondimensional film thickness at equilibrium = 0.0246. Polar case with apolar support.

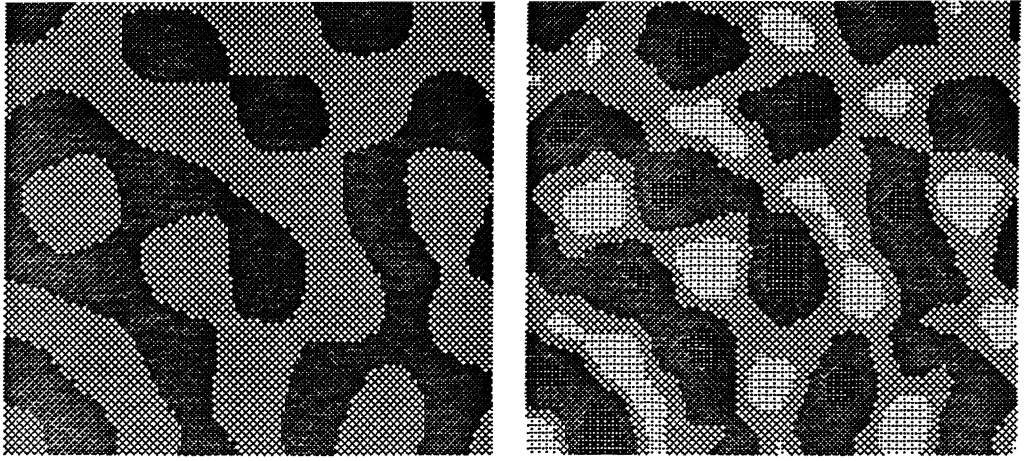

(A) (B)

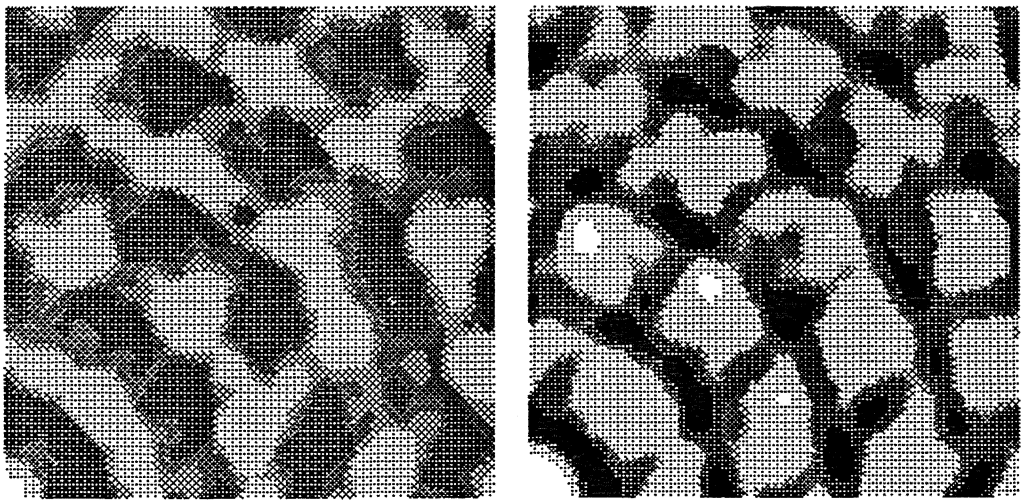

(C) (D)

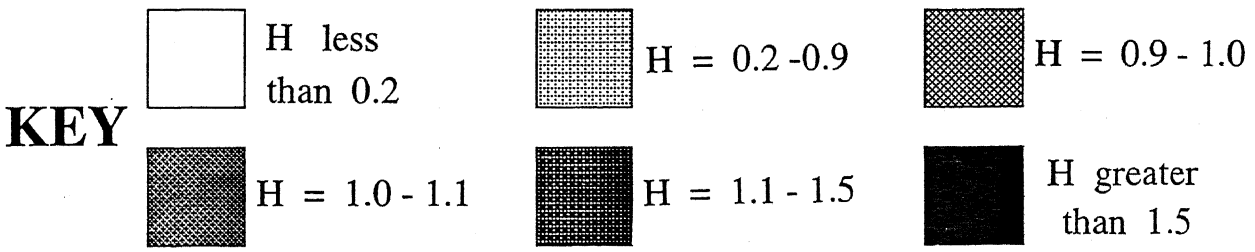

Fig. 2.11 The contour plots for the 3D configurations of the selected curves of fig. 1.10 drawn for $4\Lambda_m : 4\Lambda_m$. The fig (A), (B), (C), and (D) respectively correspond to the curves 1,2,4, and 6 of fig. 1.10.

They are supposed to be important in multilayer adsorption and heterogeneous nucleation (19). Since the consideration of nonlinear dynamics of the films for two dimensional perturbation in a large domain is difficult with the present computational facilites, the method of superposition of waves with random phase shifts and orientation (22) is adopted to generate these structures. At any point in xy plane, the net contribution to the film thickness (H_T) by M number of waves of constant wavelength, which are randomly oriented and phase shifted, can be written as:

$$H_T = \sum_{j=1}^{M} f\left[K\left(x\cos\theta_j + y\sin\theta_j\right) + \phi_j\right] \tag{2.38}$$

where θ_j is the orientation of the jth wave, ϕ_j is its phase shift and K is the wave number which is constant for all of these waves. The contribution of each of these waves can be obtained from the information available for the x vs H (simulated film thickness) profile using its periodic property and suitable interpolation technique. Then the film thickness at the said point can be estimated by dividing H_T with a suitable scaling factor (SF). SF can be calculated from the mass conservation principle as given by:

$$SF = \frac{\overline{H}_T}{\overline{H}} \tag{2.39}$$

Here $\overline{H}_T$ is the mean value of H_T, calculated by using H_T values for all the points considered in the xy plane. $\overline{H}$ is the mean value of the film thickness H, obtained from the simulation.

The four snap shots at different time show how the small holes are developed and then propagated to produce larger ones. To describe it more clearly, fig.(2.11A) shows the condition at initial perturbation. Then the second one

(fig.2.11B) shows the intermediate evolution containing larger variation in the local film thickness, as is evident from the increase in the number of shades than in the previous one. The third figure (fig.2.11C) corresponds to the two drops configuration in two dimension. It shows larger holes (increased depth and width) because of the appearance of two more shades and the reduction of the area occupied by the initial two shades. Fig.(2.11D), corresponding to the equilibrium profile, gives these holes with much larger dimensions since the effect on the shades, as discussed for the third figure, is more prominent here.

The last part of the results for this case, as shown in fig.(2.12), deals with the evolution of a random perturbation for the same values of h_0 and γ as in the previous result. The initial and final profiles are shown for a length proportional to that of three unit cells. The stabilizing nature of the system is more confirmed in this case.

- POLAR SUBSTRATE:

Only one parameter study is shown for this subgroup as the other ones are almost same as those in the previous case. Fig.(2.13) shows the variation of the equilibrium profiles for different h_0 at constant interfacial tension. The only interesting thing can be discussed here is that the thin film structure in the ultimate profiles are almost in the order of the original mean thickness. The other features can be explained similarly as in the previous case.

2.7 CONCLUSION AND RECOMMENDATIONS

It can be concluded that, for low interfacial tension cases bending moment has an important role in the film stability and hence has to be incorporated to study the cell-support adhesion phenomena. With bending moment and interfacial tension

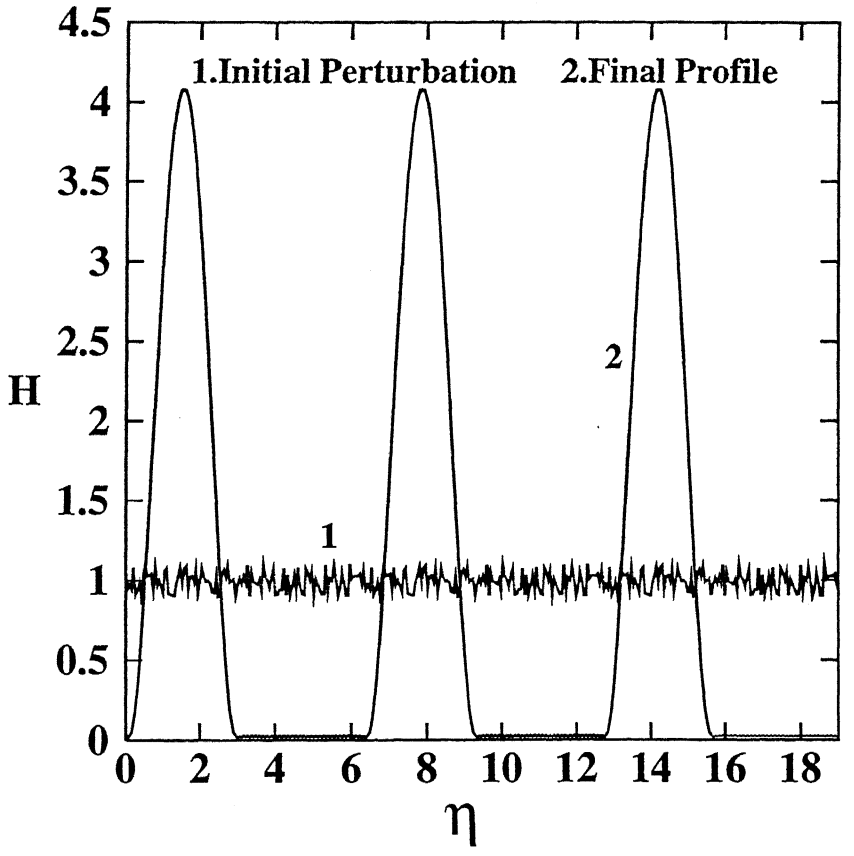

Fig. 2.12 The initial and final profiles for a random purturbation. The all parameter values are same as in fig. 1.10. The figure is drawn for $3\Lambda_m$. Minimum nondimensional film thickness = 0.025. Nondimensional time of equilibriation = 10. Polar case with apolar support.

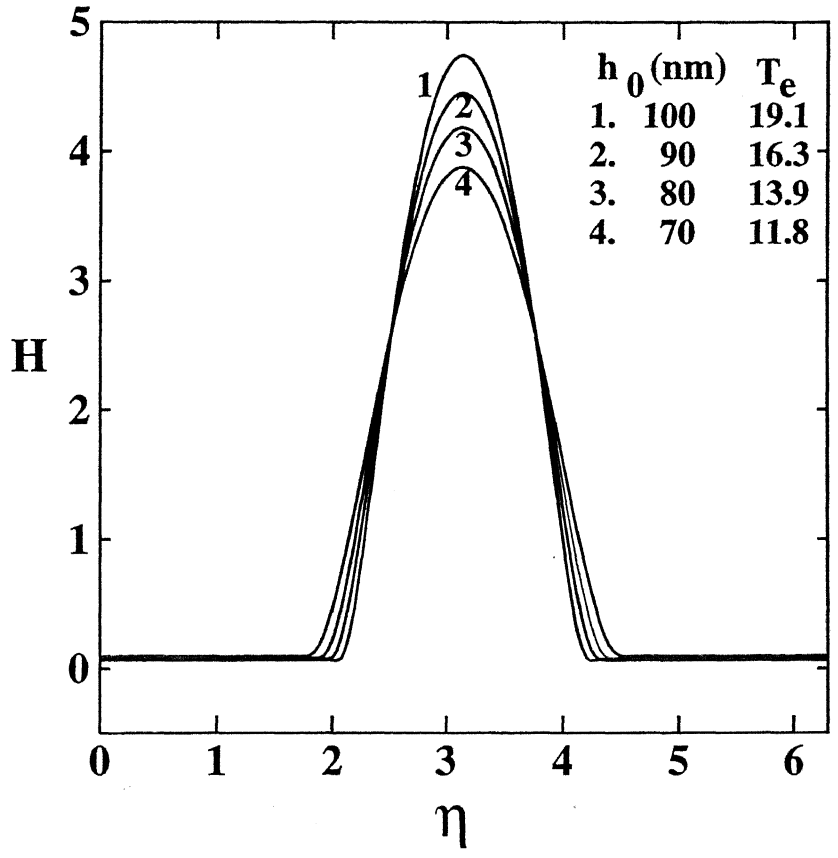

Fig. 2.13 Nondimensional equilibrium profiles for different mean film thickness. Polar case with polar support. Interfacial tension is 0.001 mJ/m^2. $S^{LW} = -4mJ/m^2$ and $S^{AB} = 25mJ/m^2$. The values of A, nondimensional minimum film thickness and nondimensional dominant wavelengths are given as - Curve 1: 4.08, 0.061, 18.34 ; Curve 2: 3.31, 0.072, 16.67 ; Curve 3: 2.61, 0.083, 15.06 ; Curve 4: 2.0, 0.098, 13.54.

together, the qualitative results do not change much from the case of instability study for the gas-liquid film interface. But quantitatively for different values of interfacial tension, the results have shown a large varitation, specially for the length scale of instability and the ultimate structure of the cell-film interface at the time of equilibriation or rupture. This is expected since interfacial tension has stabilizing effect on the film. The time scale variations can be neglected as they are micro seconds phenomena. So these cell membranes evolve in a larger length scale to form a more stabilized ultimate configuration.

From the observations of this chapter it can be proposed that, to study the physics of this type of systems, one may include other effects like Marangoni effect, the effect of presence of some specific molecules on the membrane surface etc., together with the effect of bending moment to get a more realistic result, according to the nature of the study. One can also include the effect of Born repulsion (23), but it may not be useful as the system is originally stable for most of the cases discussed above. Another important thing to be noted is that for low surface tension and highly curved surface structural effect, like the existence of a structural double layer can play an important role in the interfacial instability. Further work may be carried out in this respect with the complete stability analysis of highly curved and charged films (5). Since the resulting profiles developed in case of the bending moments are quite interesting and varying for different cases, in order to visualise their three dimensional form actual three dimensional analysis may be done, instead of the statistical estimation of those structures presented here.

Chapter 3

EFFECT OF RECEPTOR AGGREGATION ON THE MEMBRANE SURFACE IN THE PROCESS OF CELL-SUBSTRATE ADHESION

3.1 INTRODUCTION

In the study of cell adhesion on a solid support another important aspect is the presence of specific molecules on the surface of the cell-membrane called receptors. It has been proposed by several workers (2,9,24) that at the moleculer level cell adhesion to the support may be mediated by a wide variety of adhesion molecules, termed as receptors, interacting with a broad spectrum of exogenous surfaces. They are also thought to be possessing adhesive properties with respect to some specific sites on the solid support. In the present work this particular concept is viewed in the light of modified specific interactions between the membrane and the support due to the presence of receptors. The receptors try to aggregate at some points or other on the membrane under the influence of both

ordinary diffusion and convection caused by local membrane curvature. This aggregation in some cases may change the original interaction properties of the bare membrane, resulting in a different type of system behaviour. Here a model is proposed to modify the interaction potential and thus the corresponding terms in the governing equations of the system (evolution equation for the membrane-film interface and mass balance equation for the receptors). Using proper techniques, numerical experiments are carried out for some specific cases to validate the above proposition.

3.2 MODELING OF INTERACTION POTENTIAL IN PRESENCE OF RECEPTORS

The basic tenet for this modeling is that the receptors can aggregate and change the potential of the membrane locally. At some points the receptor concentration (Γ) becomes maximum. The other limit is the value for the bare membrane at $\Gamma = 0$. The behaviour can be thought of being linear initially, and after some certain value of Γ, becomes asymptotic when the modified potential of the membrane is close to that of the receptors. Mathematically this can be expressed by the following equation:

$$\triangle G = \triangle G_m + \frac{(\triangle G_r - \triangle G_m)\,\Gamma}{C + \Gamma} \tag{3.1}$$

where $\triangle G_m$ is the free energy change for the bare membrane and $\triangle G_r$, that for the receptors. C is the modeling parameter which dictates the value of Γ_∞. The variable $\triangle G$ is the modified free energy change for the system which is equivalent to the spreading coefficient described in Chapter 1. Similarly the values of $\triangle G_m$ and $\triangle G_r$ can be evaluated from the corresponding data of interfacial tensions, as in Chapter 1. The above equation [3.1] can be used for both the LW and AB

components of the free energy.

3.3 FORMULATION

The basic system discussed here is same as that in Chapter 1, except that the cell membrane now contains some receptor molecules which can interact with some binding sites on the solid support (fig.3.1) . The extra body force coming into play here (other than those stated in the previous chapter) is the attractive force between the receptor molecules and the binding sites. This force modifies the general definition of the body force term in the Navier-Stokes equation.

Starting from a reference state with an undisturbed film of thickness h_0 and receptor concentration of Γ_0 (number of receptor molecules per unit area), the dynamics of the system can be modelled by using N-S equation and modified continuity equation to predict the variation of Γ. A long wave analysis is done as before to get the evolution equation as follows:

$$h_t + \frac{1}{12\mu}\left(\gamma h^3 h_{xxx} - h^3\phi_x\right)_x = 0 \tag{3.2}$$

where the meaning of each term is the same as the Chapter 1. However, unlike the ϕ in Chapter 1, here ϕ is a function of both h and Γ . So ϕ can be expressed as follows:

$$\phi = -\frac{2\triangle G^{LW} d_o^2}{h^3} - \frac{\triangle G^{AB}}{l_0}\exp\left(\frac{d_0 - h}{l_0}\right) \tag{3.3}$$

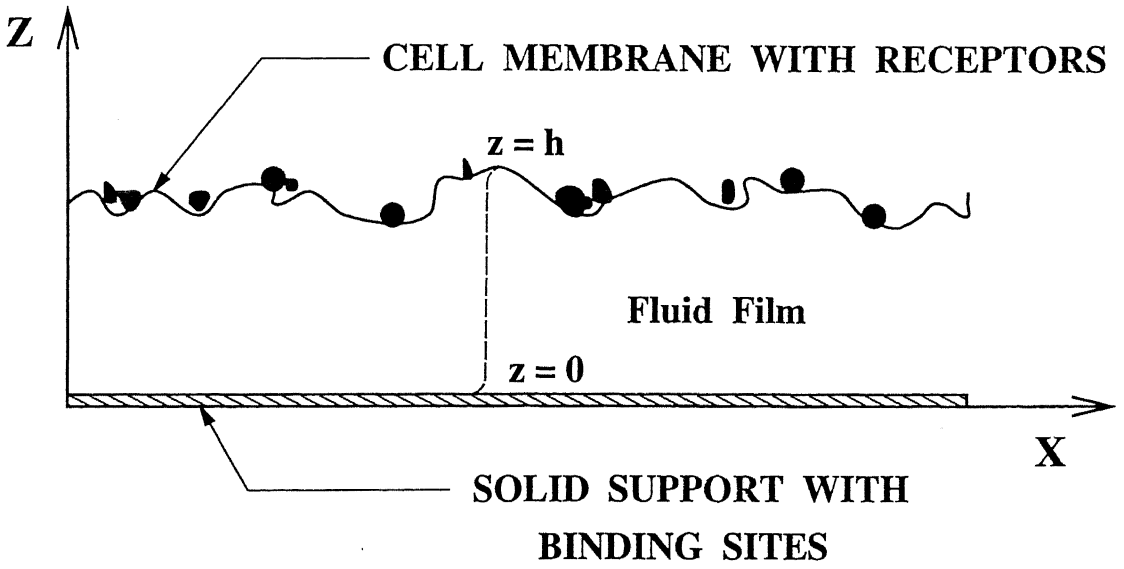

Fig. 3.1 Configuration of the system

where $\triangle G^{LW}$ and $\triangle G^{AB}$ are functions of Γ, given, in general, by equation [3.1]. Considering this functional relation of ϕ, the above evolution equation [3.2] can be modified as:

$$h_t + \frac{1}{12\mu}\left[\gamma h^3 h_{xxx} - h^3\left(\phi_h h_x + \phi_\Gamma \Gamma_x\right)\right]_x = 0 \tag{3.4}$$

The mass balance (convection-diffusion) equation for the receptor is given as follows

$$\Gamma_t = D_S \Gamma_{xx} + \left(\frac{\Gamma a_i}{f}\left(G_r\right)_x\right)_x \tag{3.5}$$

where D_S is the mass diffusion coefficient of the receptor molecules, a_i is the area occupied by each receptor molecule (surface coverage), f is the friction factor, and G_r is the total free energy for the receptors. f is defined as the ratio of KT/D_S where K is the Boltzman constant and T is absolute temperature of the system. G_r is given by the following equation:

$$G_r = \frac{\triangle G_r^{LW} d_0^2}{h^2} + \triangle G_r^{AB} \exp\left(\frac{d_0 - h}{l_0}\right) \tag{3.6}$$

where $\triangle G_r$ can be defined as the change in free energy of the receptors. $\left(G_r\right)_x$ can be substituted by $\left(G_r\right)_h h_x$.

The first term in equation [3.5] is the diffusive term and the second one is the convective term. The driving force per molecule is given by $-(G_r)_x$. So the total force for all the molecules can be obtained as $-\Gamma a_i (G_r)_x$. The total force is then divided by the friction factor to obtain the velocity. In this way the convective nature of the second term can be explained.

- NON-DIMENSIONALISATION OF THE EQUATIONS

The above equations are non-dimensionalised to give

$$H_T - \left[sgn\left(\triangle G_m^{LW}\right) \left\{ \frac{1}{H} \left(1 + \frac{\overline{G^{LW}}}{\left(\frac{\overline{C}}{\overline{\Gamma}}+1\right)} \right) - A_1 H^3 \exp\left(\frac{d-h}{l}\right) \left(1 + \frac{\overline{G^{AB}}}{\left(\frac{\overline{C}}{\overline{\Gamma}}+1\right)} \right) \right\} H_X \right]_X$$
$$+ \left[sgn\left(\triangle G_m^{LW}\right) \left\{ \frac{A_2}{\left(\overline{C}+\overline{\Gamma}\right)^2} - \frac{A_3 H^3}{\left(\overline{C}+\overline{\Gamma}\right)^2} \exp\left(\frac{d-h}{l}\right) \right\} \overline{\Gamma}_X + H^3 H_{XXX} \right]_X = 0 \tag{3.7}$$

$$\overline{\Gamma}_T = A_6 \left[A_4 \overline{\Gamma}_{XX} - sgn \triangle G_r^{LW} \left\{ \overline{\Gamma} \left\{ \frac{1}{H^3} - A_5 \exp\left(\frac{d-h}{l}\right) \right\} H_X \right\}_X \right] \tag{3.8}$$

The following non-dimensional parameters are defined:

$$X = \frac{a}{h_0} x,\ T = \frac{\nu}{h_0^2} bt,\ H = \frac{h}{h_0},\ \overline{\Gamma} = \frac{\Gamma}{\Gamma_0}$$
$$d = \frac{d_0}{h_0},\ l = \frac{l_0}{h_0} \tag{3.9}$$

where $\nu = \frac{\mu}{\rho}$. The definitions of a and b are as follows:

$$a = \sqrt{\frac{6 d_0^2 \left|\triangle G_m^{LW}\right|}{\gamma h_0^2}},\ b = \frac{\left(6 d_0^2 \left|\triangle G_m^{LW}\right|\right)^2}{12 \mu \nu \gamma h_0^3} \tag{3.10}$$

Other dimensionless constants are given by:

$$\overline{C} = \frac{C}{\Gamma_0},\ \overline{G}^{LW} = \left(\frac{\triangle G_r^{LW}}{\triangle G_m^{LW}} - 1 \right),\ \overline{G}^{AB} = \left(\frac{\triangle G_r^{AB}}{\triangle G_m^{AB}} - 1 \right) \tag{3.11}$$

$$A_1 = -\frac{h_0^4 \triangle G_m^{AB}}{6 d_0^2 l_0^2 \triangle G_m^{LW}},\ A_2 = \frac{C\overline{G}^{LW}}{3\Gamma_0},$$

$$A_3 = -\frac{\Gamma_0 h_0^3 \left(\triangle G_r^{AB} - \triangle G_m^{AB}\right)}{6 C l_0 d_0^2 \triangle G_m^{LW}},\ A_4 = \frac{f D_S h_0^2}{2 a_i d_0^2 |\triangle G_r^{LW}|}, \tag{3.12}$$

$$A_5 = -\frac{h_0^3 \triangle G_r^{AB}}{2 l_0 d_0^2 \triangle G_r^{LW}},\ A_6 = \frac{4 a_i \mu |\triangle G_r^{LW}|}{h_0 f |\triangle G_m^{LW}|}$$

The six constants A_1 to A_6 [3.12] help to understand the behaviour of the equations [3.7] and [3.8]. A_1 shows the relative effect of the LW and AB forces for the bare membrane. A_2 and A_3 govern the effect of the receptors, A_3 describes the polar contribution of the receptors. A_4 shows the relative effect of the diffusive part compared to the convective part in the mass balance and A_5 has similar effect as that of A_1 in the convective part. A_6 has the important role of predicting the time scale of aggregation of the receptor molecules. The other two constants $\overline{G}^{LW}$ and $\overline{G}^{AB}$ couple the potential field of the receptors with that of the bare membrane. In all, the term in the first braces in equation [3.7] has stabilizing or destabilizing effect depending on the values of $\mathrm{sgn}\left(\triangle G_m^{LW}\right)$, A_1, $\overline{G}^{LW}$ and $\overline{G}^{AB}$. The first term in the second braces shows the effect of stabilization or destabilization depending on the values of $\mathrm{sgn}\left(\triangle G_m^{LW}\right)$, $A_2$and A_3. These two terms are coupled by the parameters H and $\overline{\Gamma}$ and their respective derivatives. In the mass balance equation [3.8] the first term is diffusive and the one in the braces is convective.

3.4 LINEAR STABILITY ANALYSIS

As in Chapter 1, the two governing equations for the overall system [3.7] and [3.8] can be linearised around the mean values of h and Γ (i.e. h_0 and Γ_0). In that case the solution of the nondimensional evolution equation can be written as follows:

$$H = 1 + E_h \exp(iKX + \Omega T) \tag{3.13}$$

and that for the nondimensional mass balance equation is of the form:

$$\overline{\Gamma} = 1 + E_\Gamma \exp(iKX + \Omega T) \tag{3.14}$$

where E_h and E_Γ are the nondimensional amplitudes of the perturbations applied to the system given by:

$$E_h = \frac{\epsilon_h}{h_0}, \; E_\Gamma = \frac{\epsilon_\Gamma}{\Gamma_0} \tag{3.15}$$

where ϵ_h and ϵ_Γ are the dimensional amplitude of perturbations. K is the wave number and Ω is the growth rate of the perturbations in nondimensional form.

Now using these solutions, equations [3.7] and [3.8] can be linearised to give the expression for E_Γ and Ω in terms of the nondimensional constants (shown before) and the wave number K as follows:

$$E_\Gamma = \frac{A_6 sgn\left(\triangle G_r^{LW}\right)\left(1 - A_5 \exp\left(\frac{d-1}{l}\right)\right) E_h K^2}{\Omega + A_4 A_6 K^2} \tag{3.16}$$

$$\Omega^2 + c_1\Omega + c_2 = 0 \tag{3.17}$$

where c_1 and c_2 are given by:

$$c_1 = K^2\left[K^2 + sgn\left(\triangle G_m^{LW}\right)\left\{\left(1 + \frac{\overline{G}^{LW}}{\overline{C}+1}\right) - A_1 \exp\left(\frac{d-1}{l}\right)\left(1 + \frac{\overline{G}^{AB}}{\overline{C}+1}\right)\right\} + A_4 A_6\right] \tag{3.18}$$

$$c_2 = A_4 A_6 K^4 \left[K^2 + sgn\left(\triangle G_m^{LW}\right) \left\{ \left(1 + \frac{\overline{G}^{LW}}{\overline{C}+1}\right) - A_1 \exp\left(\frac{d-1}{l}\right) \left(1 + \frac{\overline{G}^{AB}}{\overline{C}+1}\right) \right\} \right]$$
$$+ \frac{A_6 K^4}{\left(\overline{C}+1\right)^2} sgn\left(\triangle G_m^{LW}\right) sgn\left(\triangle G_r^{LW}\right) \left(1 - A_5 \exp\left(\frac{d-1}{l}\right)\right) \left(A_2 - A_3 \exp\left(\frac{d-1}{l}\right)\right) \tag{3.19}$$

The expression for the nondimensional amplitude of receptor perturbation implies that for the cases with attractive van der Walls force, the evolution of receptor concentration will be just the opposite of that for the film thickness. So larger concentration will be found at the smaller film thickness, which will significantly affect the free energy change at those points. The Ω has two roots of which only the positive one is responsible for the instability. The value of K corresponding to the maximum value of Ω gives an estimate for the wave number of the fastest growing wave. The set of values of Ω and K for this case can be used to obtain the linear time of rupture as shown in Chapter 1.

3.5 NON-LINEAR ANALYSIS

The linear theory only gives the estimate of the initial (upto which the system is fairly linear) behaviour for any system. So the better way to study the physics of the system is by using the nonlinear approach. The observations are broadly divided into two parts. In one case the system containing bare membrane along with the film and the support is originally apolar, and in the other case it is polar.

NUMERICAL METHOD

Here the method of solution of the two coupled partial differential equations is almost same as that in Chapter 1, except that for the purpose of discretization the approach of finite difference is adopted instead of Fourier collocation technique. The reason of this change is that the system becomes highly nonlinear after some time at some specific locations. This needs high grid density for these locations. Use of Fourier collocation for such high number of grid points is very time consuming and at the same time gives erroneous result.

The concept of finite difference used here is given below:

$$(Y_X)_i = \frac{Y_{i+\frac{1}{2}} - Y_{i-\frac{1}{2}}}{\triangle X} \tag{3.20}$$

where Y is any fuction value and Y_X is derivative of Y with respect to X at the ith grid point. The necessary function values at the $i+\frac{1}{2}$ and $i-\frac{1}{2}$ grid points are interpolated using suitable technique. Like in Chapter 1, here also the inital condition is taken from the solution of the linear stability analysis at $T = 0$ and periodic conditions are used as the boundary conditions.

3.6 RESULTS AND DISCUSSION

To obtain the results for different cases considered so far, the specific parameter values for the system are taken to be of the same order as those used in Chapter 1. The free energy values for the receptors for both LW and AB are also considered to be of the same order as those of bare membranes. Here two specific cases are considered regarding the bare membrane to make a comparative study : firstly, the apolar case with strong apolar attraction of van der Waals force and no polar part, and secondly, the more interesting one, the polar case where the van der Waals attraction together with the repulsive polar components are present. The actual values of the free energy change (spreading coefficients) in these two

cases for membrane, used in computaion, are shown in table (3.1). The receptor potential considered for these two cases are same, given by $\Delta G_r^{LW} = -4$ mJ/m^2 and $\Delta G_r^{AB} = -45$ mJ/m^2, that is, both the components are destabilizing in nature. The values of the parameters (7) other than those used in Chapter 1 are summarised in table (3.2). The values of a_i and $\overline{C}$ are varied to get different set of results for each of the above two cases.

At first linear analysis is done for both the cases to get the values of K_m for them. The variation of Ω with K and h_0 for the two cases is shown in fig.(3.2). For the apolar case, the disturbance is maximum at small values of h_0. On the other hand, for the polar case this is observed for h_0 around 9 nm . To draw a better comparision of the results of polar and apolar cases, h_0 is assigned a value of 10 nm (at which the instability for the polar case is the least among the values shown in fig.(3.2)) in both the cases.

For the nonlinear results, the grid convergence study is done at first. The comparative results for the polar case with 400 and 800 grid points in the full wavelength are shown in fig.(3.3). It shows the ultimate h and Γ profiles. The results for the two sets of grid points are fairly similar except for the values of $\Gamma_{\max}$. The time taken to reach this condition is also almost same for these two cases. Though the profiles for the 800 grid points are smoother, but this requires approximately triple the computational time. So for each of the two cases stated above, only one set of results will be presented with 800 grid points later.

The results of the nonlinear simulation for the apolar case is shown in figs.(3.4) and (3.5) for one set of values of a_i and $\overline{C}$. The LW component of free energy for the bare membrane is taken here to be double of that for the receptors, to make the system highly apolar in nature. Fig.(3.4) shows the variation of the minimum film thickness and maximum receptor concentration with time and fig.(3.5) shows

Table 3.1: The values of different components of free energy in mJ/m^2 for the bare membrane

	LW Component	**AB Component**
Apolar Case	-8	0
Polar Case	-4	25

Table 3.2: Estimated parameter values

Parameter	**Best estimates**
Absolute Temperature	298 K
Viscocity of film-fluid	0.8 cp
Surface diffusion coefficient	10^{-13} m^2/s
Surfactant concentration	$10^{12} - 10^{15}$ molecules/m^2
Surface Coverage of surfactant	10-1000 $(nm)^2$

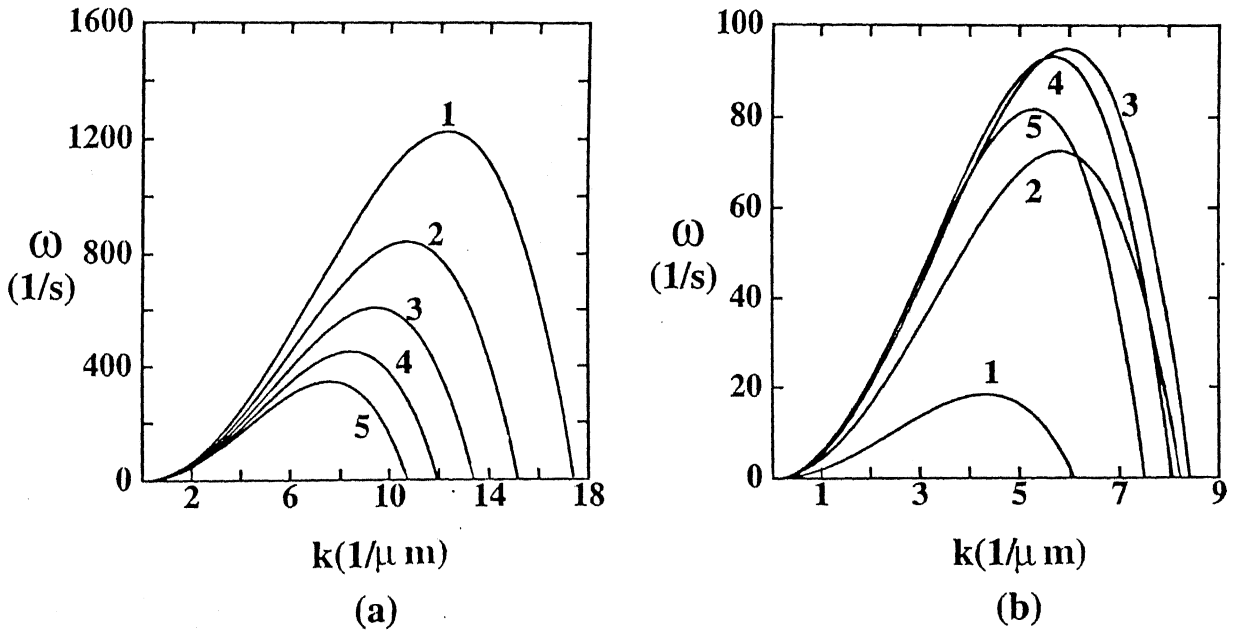

Fig.3.2 Variation of dimensional growth rate with dimensional wave number for different values of h_0. For receptor $\Delta G^{LW} = -4mJ/m^2$ and $\Delta G^{AB} = -45mJ/m^2$. (a) Apolar case, i.e., for bare membrane $\Delta G^{LW} = -8mJ/m^2$ and $\Delta G^{AB} = 0$. (b) Polar case, i.e., for bare membrane $\Delta G^{LW} = -4mJ/m^2$ and $\Delta G^{AB} = 25mJ/m^2$. Values of a_i and $\overline{C}$ are 10 nm^2 and 2, respectively. For curves 1 to 5, h_0 values are 8, 8.5, 9, 9.5, 10 nm, respectively. Interfacial tension is the stabilising factor.

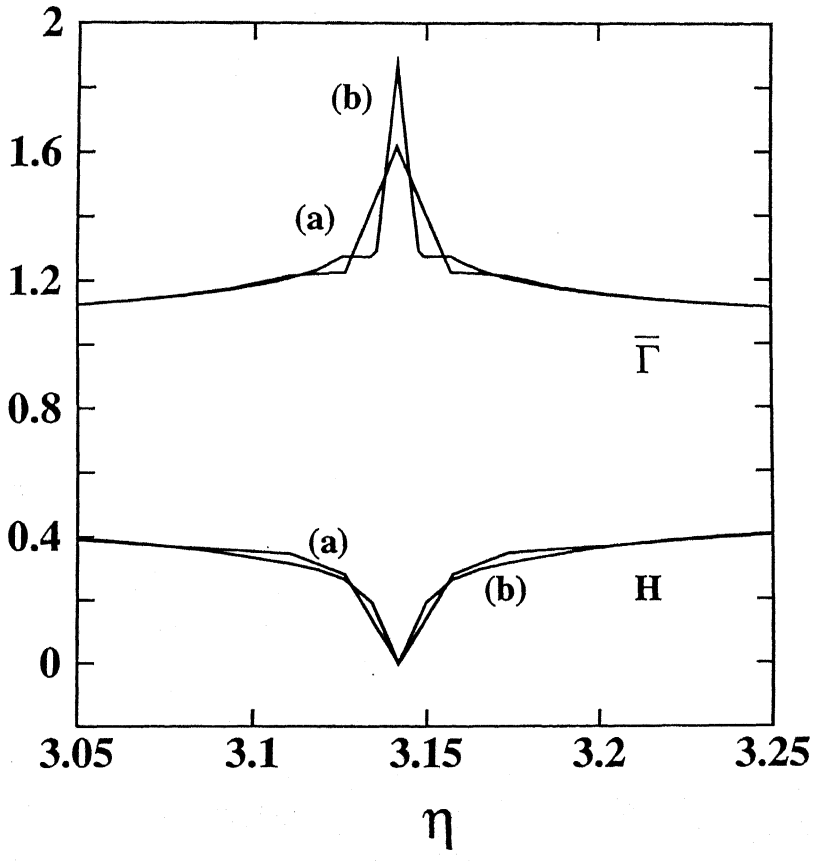

Fig. 3.3 Nondimensional profiles at the time of rupture for (a) 400 grid points, and (b) 800 grid points. Polar case with h_0 = 10 nm. Other parameter values are same as in polar case of fig.3.2.. Interfacial tension is the stabilising factor.

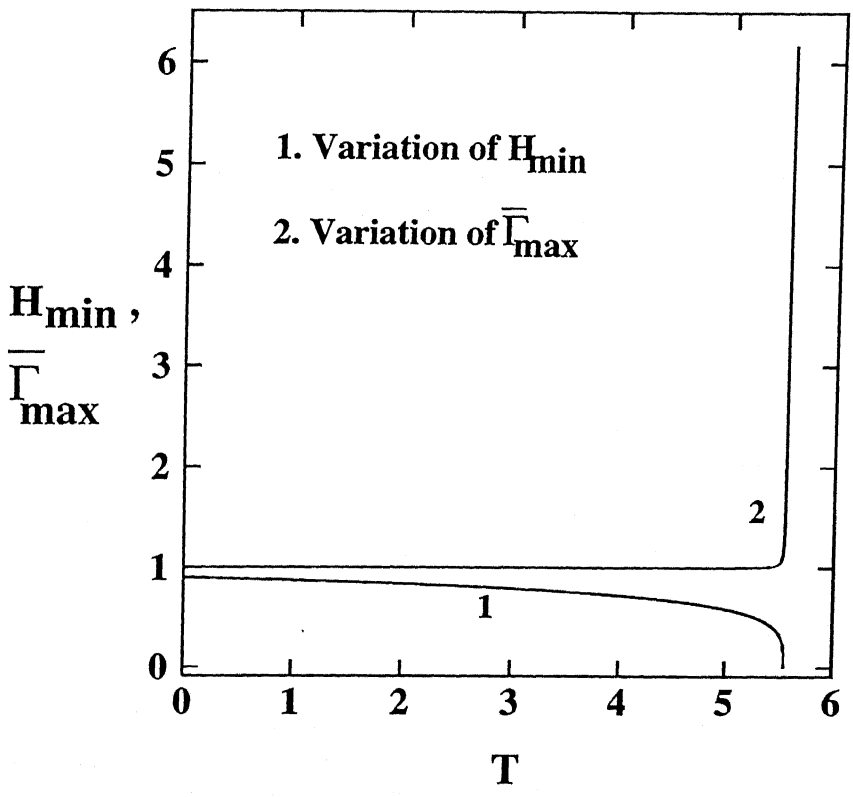

Fig. 3.4 Variation of nondimensional minimum film thickness and maximum receptor concentration with nondimensional time. Apolar case with $h_0 = 10$ nm. Other parameter values are same as in apolar case of fig.3.2 .Interfacial tension is the stabilising factor.

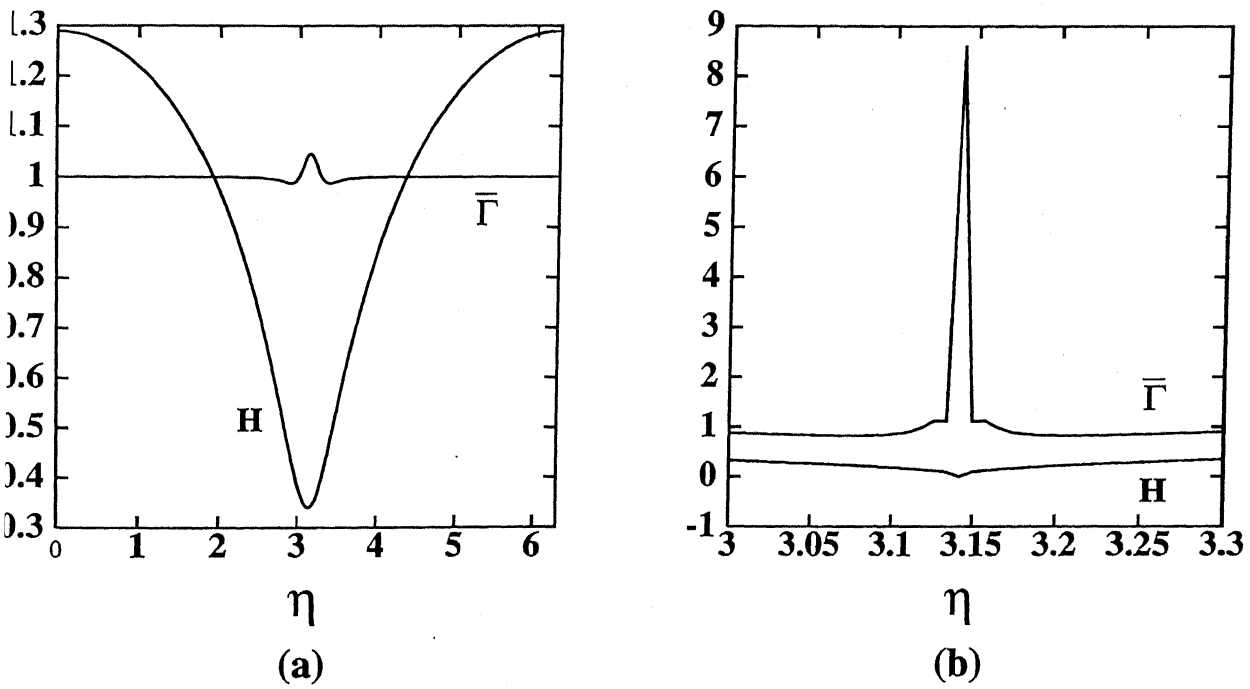

Fig. 3.5 Nondimensional profiles at and just before rupture. (a) just before rupture and (b) at the time of rupture. Apolar case with $h_0 = 10$ nm. Other parameter values are same as in apolar case of fig.3.2. Interfacial tension is the stabilising factor.

the profile of the film thickness and receptor-concentration just before and at the time of rupture. It is clear from these figures that the receptor aggregation has no effect on the film stability. For both the cases with and without receptors, the film ruptures. However, quantitavely, just before the rupture, due to high gradient of the film thickness with the length, near the point of rupture the receptor concentration increases (fig (3.5a)). This accelerates the process of rupture and the receptor concentration shoots up to a high value compared to the mean concentration at and around the point of rupture. So on the whole, in this case the receptors cannot affect the bare membrane potential so much as to change the process of cell adhesion (both the dynamics and equilibrium solution) on the support. The experiments for the other combinations of a_i and $\overline{C}$ show that they can only change the maximum receptor concentration at the time of rupture and the time of rupture itself.

The results of the nonlinear studies for the polar case is interesting. Here the LW component of the free energy for both the bare membrane and the receptors is taken to be the same in magnitude and sign to decouple the effect of receptors on the AB component of the free energy for the system. As shown by some workers, the film always attains an equilibrium profile, made up with ultrathin film and drop(s), in those cases where LW and AB components of free energy are opposite in nature (17,19). The same observation may be extended for the case of bare membrane system with same type of potential, as is found in the previous chapter. But the results with receptors show that the film ruptures and hence the actual contact of cell and support becomes possible, which is qualitatively just the opposite. This can be rationalised from the view point of receptor aggregation at some points of the membrane during its evolution. A nondimensional free energy term can be defined here by dividing equation [3.1] by ΔG_m. This can be applied

for both the LW and AB components of free energy. Since here only the effect on AB component is taken into account, it is represented in nondimensional form by:

$$\overline{\Delta G}^{AB} = 1 + \frac{\overline{G}^{AB}}{\frac{\overline{C}}{\overline{\Gamma}} + 1} \tag{3.21}$$

It can be easily identified with the second expression in the braces of the first term of equation [3.7]. The study of this term during the process of evolution will help in understanding the force field acting on the system at different instant.

With the help of fig.(3.6), (results with same set of values of a_i and $\overline{C}$ as that in the apolar case, shown in the nondimensional forms), the process of evolution for a typical case can be explained. Initially when there is no significant receptor aggregation, the membrane behaviour is similar to that of the bare membrane. The steady profile is attained after some time of the initial perturbed condition which is almost unchanged for a long time, during which the receptor aggregation takes place. This is shown by the flat region of the $H_{\min}$ curve in fig.(3.6d). The curves 2 show the condition at an intermediate time in between initial perturbation (curves 1) and the steady state profile (curves 3). The curves 3 are drawn at a specific instant during this period of time. .Upto this point there is a slow increase in the maximum value of Γ as shown by the $\overline{\Gamma}_{\max}$ curve of fig.(3.6d). Then Γ attains a high value at some point(s) on the membrane surface which further facilitates the evolution, as shown by the curves 4. The interesting difference between the $\overline{\Delta G}^{AB}$ profiles of curves 3 and 4 is that, for the latter the free energy attains negative values at some points on the membrane, which signals the recommencement of the instability. Now both h and Γ affect each other. The minimum film thickness decreases, while the maximum receptor concentration increases at that point, as shown in the curves 5 of fig.(3.6c) and

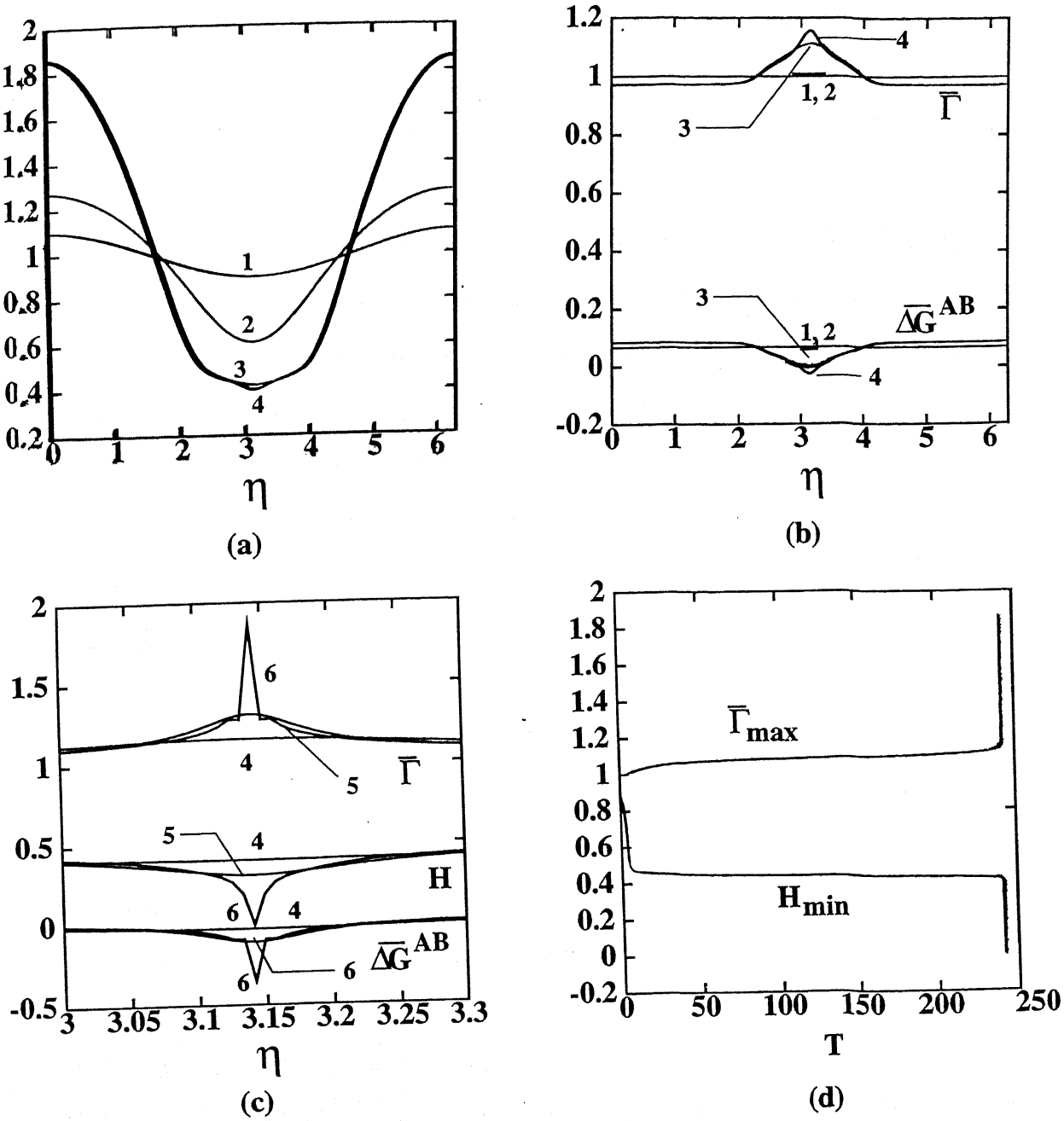

Fig. 3.6 Evolution of nondimensional profiles (a) to (c) with nondimensional time. (d) Variation of the nondimensional minimum film thickness and maximum receptor concentration with nondimensional time. Polar case with $h_0 = 10$ nm. Other parameter values are same as in polar case of fig.3.2. The nondimensional times for the curves 1 to 6 are T = 0, 8, 225, 241.4, 241.8, 241.8009, respectively. Interfacial tension is the stabilising factor.

by the rightmost parts of both of the curves in fig.(3.6d). Now the potential of the system is considerably affected by the receptor concentration which makes the change in $\triangle G$ (here only $\triangle G^{AB}$) values at some points highly negative (see curve 5). This ultimately leads the film to rupture, together with high receptor concentration at the rupture point (the curves 6).The curves obtained from the simulation result are not smooth due to less number of data points. A smoothed version of the curves 6 of fig.(3.6c) is shown in fig.(3.7).

As in the previous chapter a 3D structure is generated for the above case using the principle of random wave superposition. Three specific instants are chosen, namely, at the time when quasi-equilibrium state is attained when $\overline{\triangle G}^{AB}$ is non zero for all points, then at an instant when the finger like structure is already developed and $\overline{\triangle G}^{AB}$ is negative at those points, and at an instant just before rupture. Six snap shots are presented in fig.(3.8), the left column corresponding to the film thickness and the right one to the receptor concentration at the same instant. In fig.(3.8B) there is very small variation of receptor concentration which shows the quasi equilibrium state. In fig.(3.8D) the receptor concentration varies largely which shows that the process of aggregation starts. Also in fig.(3.8C) (corresponding to fig.(3.8D)) the film thickness attains lower values and higher values at some points or other which shows that the process of evolution again starts. Fig.(3.8F) shows black points spreaded in throughout region in a random fashion which means maximum receptor concentration at these points and hence rupture will occur at these locations. This is also supported by fig.(3.8E) which shows white regions (minimum thickness) corresponding to those black points.

A wide range of results is obtained for this case when different combinations of a_i and $\overline{C}$ are tried. As seen from equation [3.1], as $\overline{C}$ increases, $\triangle G$ (here $\triangle G^{AB}$) becomes more insensitive to the variation of $\overline{\Gamma}$. So, $\triangle G$ needs more receptor

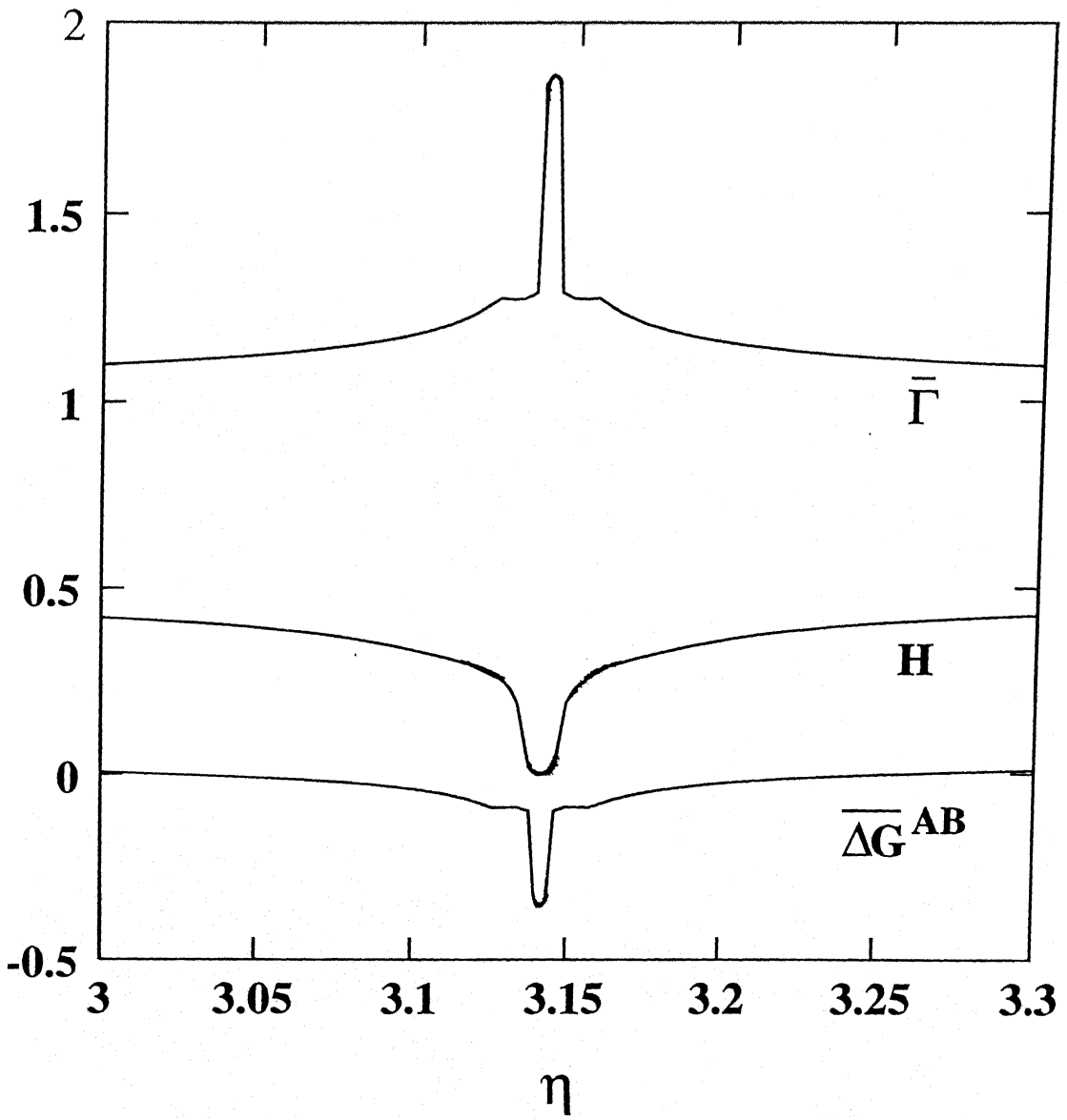

Fig. 3.7 Curves 6 of fig.3.6 after smoothing.

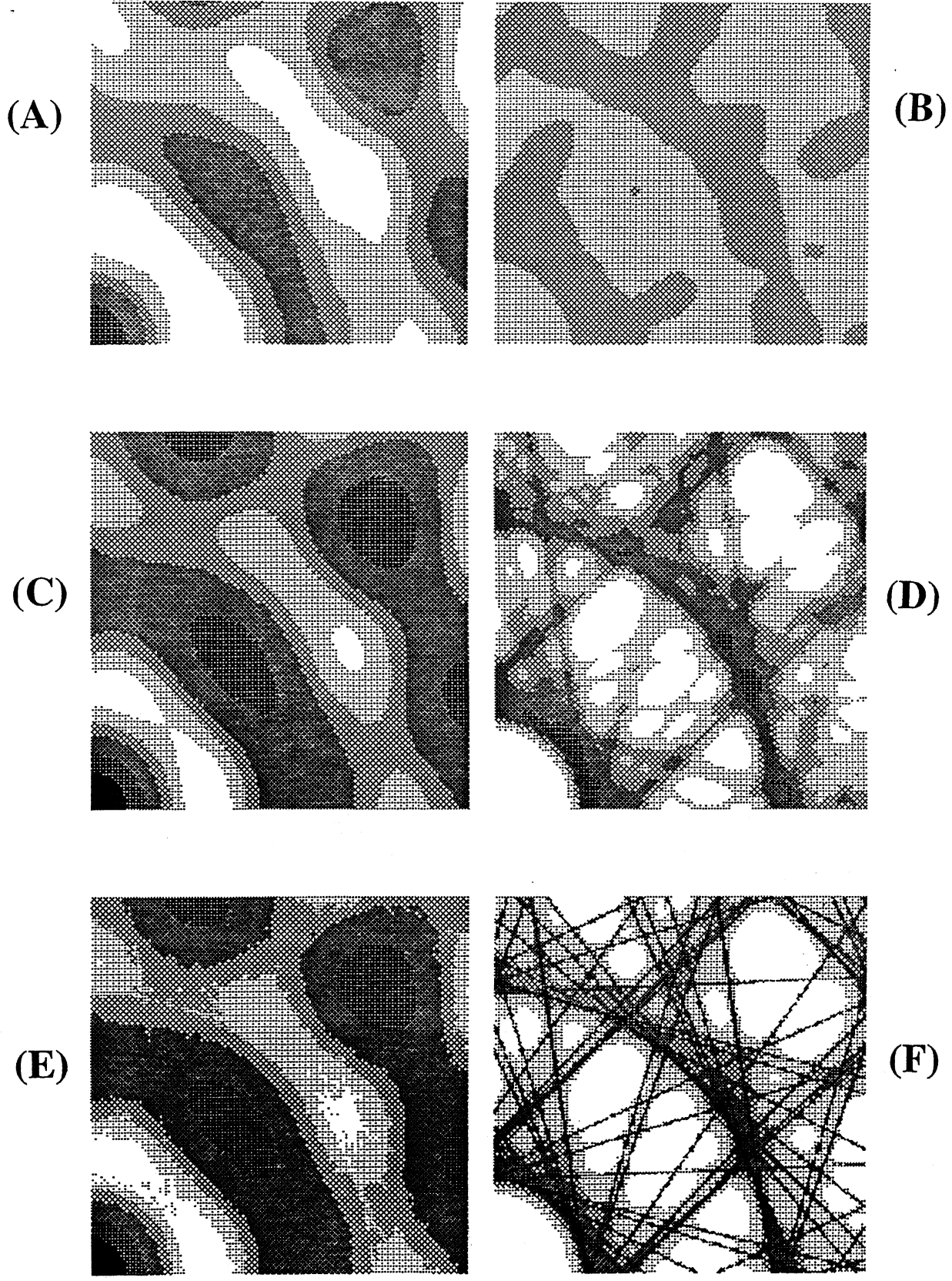

Fig. 3.8 Contour plots of the 3D profiles, estimated by using superposition of randomly oriented and phase shifted waves, for the case same as in fig.3.6. The left column for H and right one for $\overline{\Gamma}$.
(A) and (B) are at the quasi steady state. (C) and (D) are at an instant when receptor aggregation started. (E) and (F) are just before rupture. The key for the grey scale is given in fig.3.9.

Shades	H	$\overline{\Gamma}$
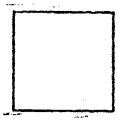	0.7 - 0.9	0.7 - 0.9
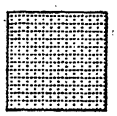	0.9 - 1.0	0.9 - 1.0
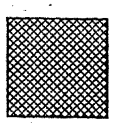	1.0 - 1.1	1.0 - 1.1
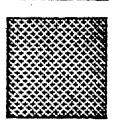	1.1 - 1.3	1.1 - 1.3
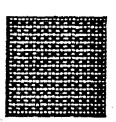	1.3 - 1.5	1.3 - 1.6
	Greater than 1.5	Greater than 1.6

Fig. 3.9 Grey scale key for the fig.3.8.

concentration to change from positive to negative value. Increase in $\overline{C}$ causes more aggregation and also prolongs the time of rupture, as is clearly seen from table (3.3). But there is a limit to which $\overline{C}$ can be increased ($\overline{C}_\infty$) for a given value of a_i, because after that receptors can no longer change $\triangle G$ significantly ($\overline{C} \gg \overline{\Gamma}$), and so another equilibrium solution is reached. This can be avoided if the amplitude of the perturbation for the receptor concentration (E_Γ) is increased (by increasing the value of a_i) so that considerable change of $\triangle G$ can occur even at high $\overline{C}$. For example, for $a_i = 160$ (nm)^2 at $\overline{C} = 2.7$ there is no rupture, whereas for the same $\overline{C}$ value at $a_i = 250$ (nm)^2 there is rupture at $T = 68$ with $\overline{\Gamma}_{\max} = 5.5$. Again, for a given $\overline{C}$, as a_i increases the receptor aggregation as well as the time required for rupture increases (table (3.3)). This is due to the fact that a_i increases the value of A_6 [3.12], which dictates the time scale of receptor-aggregation [3.8]. For a_i also, there exists a saturation value after which no significant change in rupture time or the receptor aggregation is possible.

Some interesting results are shown in fig.(3.10) to demonstrate the combined effect of a_i and $\overline{C}$ on the receptor aggregation and film instability. Their values are increased for the curves 1 to 3 shown in this figure. $\overline{\Gamma}_{\max}$ is found to increase gradually in all the cases, but the time of rupture (and hence the flat region) decreases from curve 1 to 2 and then increases again from curve 2 to 3. The decrease in flat region in curve 2 shows that for that value of a_i higher value of $\overline{C}$ can be used before $\overline{C}_\infty$ is reached. The large increase in both rupture time and maximum receptor concentration at that instant in curve 3 compared to that in curve 1 indicates the mutual reinforcing effect of these two variables. The region of the profiles where considerable changes take place near and at the time of rupture is shown for these two curves in fig.(3.11). The larger negative value of $\overline{\triangle G}^{AB}$ for curve 3 compared to that for curve 1 causes more receptor aggregation.

Table 3.3: Results from simulations with different values of a_i and $\overline{C}$

a_i $(nm)^2$	$\overline{C}$	$\overline{\Gamma}_{\max}$	T_R
160	2	3.38	5.3
160	2.2	3.67	10.28
160	2.6	4.28	893.56
170	2.6	4.38	482.65
200	2.6	4.72	68.473
250	2.6	5.3	32.7

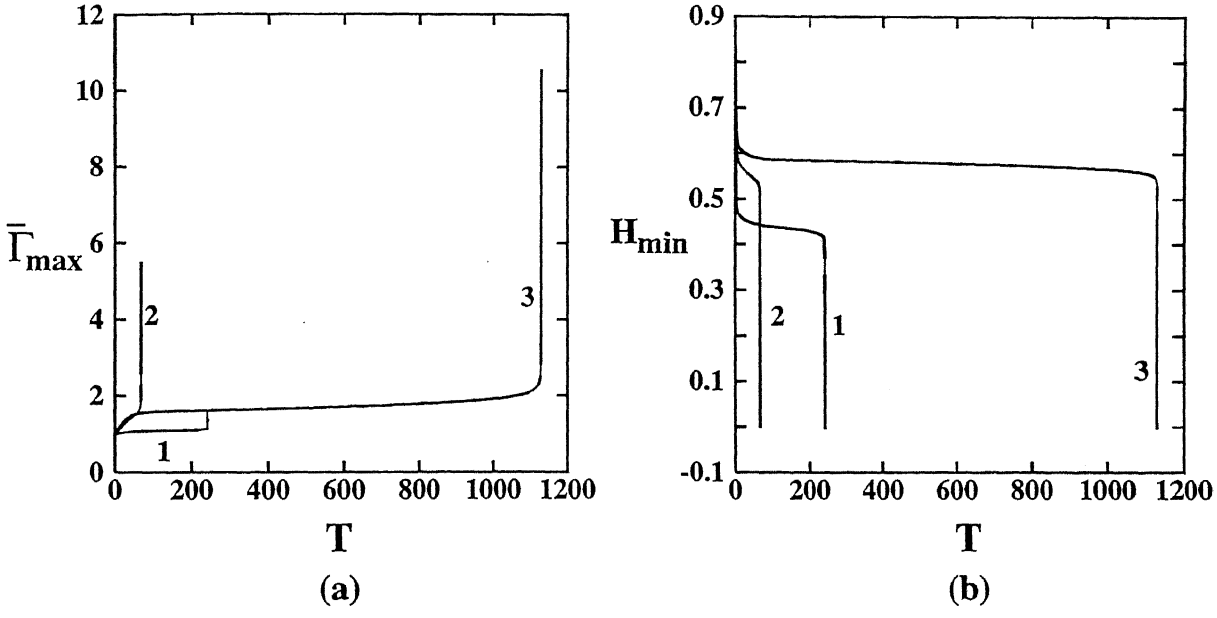

Fig. 3.10 Variation of nondimensional minimum film thickness and maximum receptor concentration with nondimensional time for different parameter values. Polar case with h_0 = 10 nm. The LW and AB components of ΔG for bare membrane and receptor are same as in fig.3.6.. Values of a_i and $\overline{C}$ for the curves 1 to 3 are respectively - Curve 1: 10 nm^2 and 2; Curve 2: 250 nm^2 and 2.7; Curve 3: 500 nm^2 and 3.3. Interfacial tension is the stabilising factor.

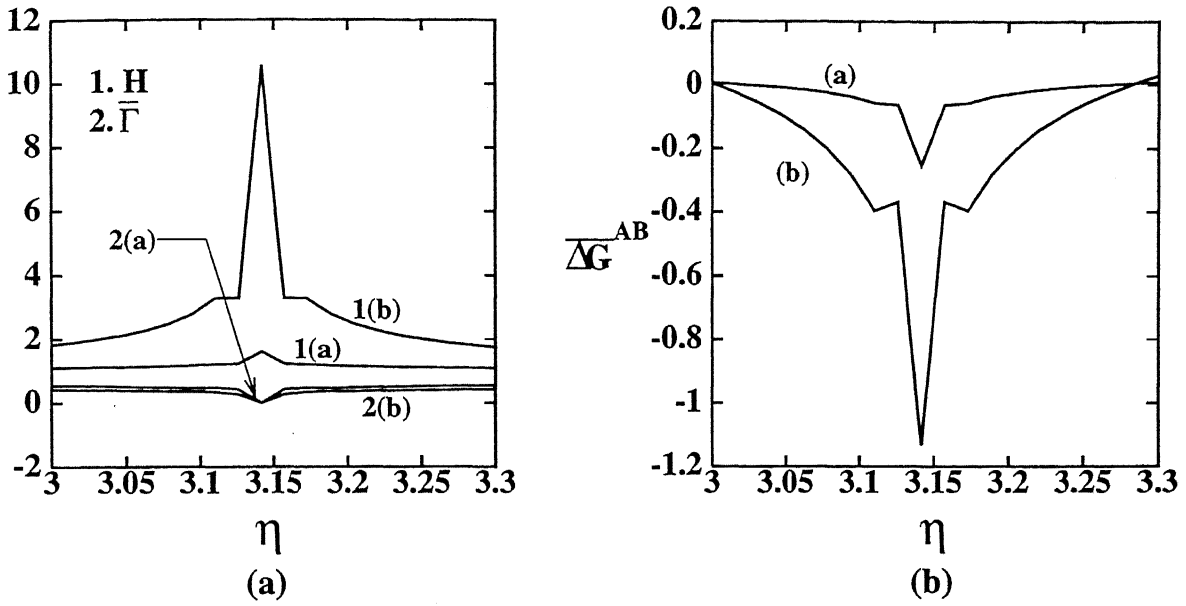

Fig. 3.11 Nondimensional profiles at the time of rupture for the curves 1 and 3 of fig.3.10.

- BENDING RESISTANCE AS STABILISING FORCE

So far, interfacial tension is considered to provide the stabilising effect to the system. As discussed in the previous chapter, this is valid for large value of interfacial tension at the membrane-film interface. But for small value of this parameter, the effect of bending resistance during the deformation of the cell has also to be taken into account. The behaviour of the system is now studied by considering the bending resistance as the only stabilising factor. The eq. [3.2] can be modified in this case as follows:

$$h_t + \frac{1}{12\mu}\left(-Bh^3h_{xxx} - h^3\phi_x\right)_x = 0 \tag{3.22}$$

The nondimensional form of the eq. [3.22] can be written as:

$$H_T - \left[sgn\left(\triangle G_m^{LW}\right)\left\{\frac{1}{H}\left(1+\frac{\overline{G^{LW}}}{\left(\frac{\overline{C}}{\overline{\Gamma}}+1\right)}\right) - A_1H^3\exp\left(\frac{d-h}{l}\right)\left(1+\frac{\overline{G^{AB}}}{\left(\frac{\overline{C}}{\overline{\Gamma}}+1\right)}\right)\right\}H_X\right]_X$$
$$+\left[sgn\left(\triangle G_m^{LW}\right)\left\{\frac{A_2}{\left(\overline{C}+\overline{\Gamma}\right)^2} - \frac{A_3H^3}{\left(\overline{C}+\overline{\Gamma}\right)^2}\exp\left(\frac{d-h}{l}\right)\right\}\overline{\Gamma}_X - H^3H_{XXXXX}\right]_X = 0 \tag{3.23}$$

where the value of space scaling parameter a will be given as:

$$a = \left(\frac{\left|6d_0^2\triangle G_m^{LW}\right|}{B}\right)^{\frac{1}{4}} \tag{3.24}$$

The other parameters and equations remain the same. From linear stability analysis the dispersion equation for this case can be wriiten similar to that of [3.17]. But the expressions of c_1 and c_2 will be as follows:

$$c_1 = K^2\left[K^4 + sgn\left(\triangle G_m^{LW}\right)\left\{\left(1+\frac{\overline{G}^{LW}}{\overline{C}+1}\right) - A_1\exp\left(\frac{d-1}{l}\right)\left(1+\frac{\overline{G}^{AB}}{\overline{C}+1}\right)\right\} + A_4A_6\right] \tag{3.25}$$

$$c_2 = A_4 A_6 K^4 \left[K^4 + sgn\left(\triangle G_m^{LW}\right) \left\{ \left(1 + \frac{\overline{G}^{LW}}{\overline{C}+1}\right) - A_1 \exp\left(\frac{d-1}{l}\right) \left(1 + \frac{\overline{G}^{AB}}{\overline{C}+1}\right) \right\} \right]$$

$$+ \frac{A_6 K^4}{(\overline{C}+1)^2} sgn\left(\triangle G_m^{LW}\right) sgn\left(\triangle G_r^{LW}\right) \left(1 - A_5 \exp\left(\frac{d-1}{l}\right)\right) \left(A_2 - A_3 \exp\left(\frac{d-1}{l}\right)\right) \tag{3.26}$$

With the help of the above modified equations, simulation is carried out for perturbation with dominant wavelength. The spreading coefficients are taken to be same as in polar case with interfacial tension. The values of a_i and $\overline{C}$ are taken as 10 $(\text{nm})^2$ and 2 respectively. 400 grid points are used, all other variables being same as in the previous case with interfacial tension. The results are shown in fig.(3.12). In this case also the receptor aggregation causes the rupture of the film and hence cell-substrate contact is made possible. Fig.(3.12a) shows the variation of $H_{\min}$ and $\overline{\Gamma}_{\max}$ with T which is similar to the curve (d) in fig.(3.6). But from fig.(3.12b) it is clear that in this case more aggregation of the receptor is needed to cause the rupture compared to the case with interfacial tension. This is due to greater stabilising effect provided by the bending resistance than the interfacial tension.

3.7 CONCLUSION AND RECOMMENDATIONS

Receptors are seen to have a significant effect in case of cell-support adhesion as is clear from the results presented above. For some specific cases their effect may be negligible (as for the apolar case), but for some, they may change the

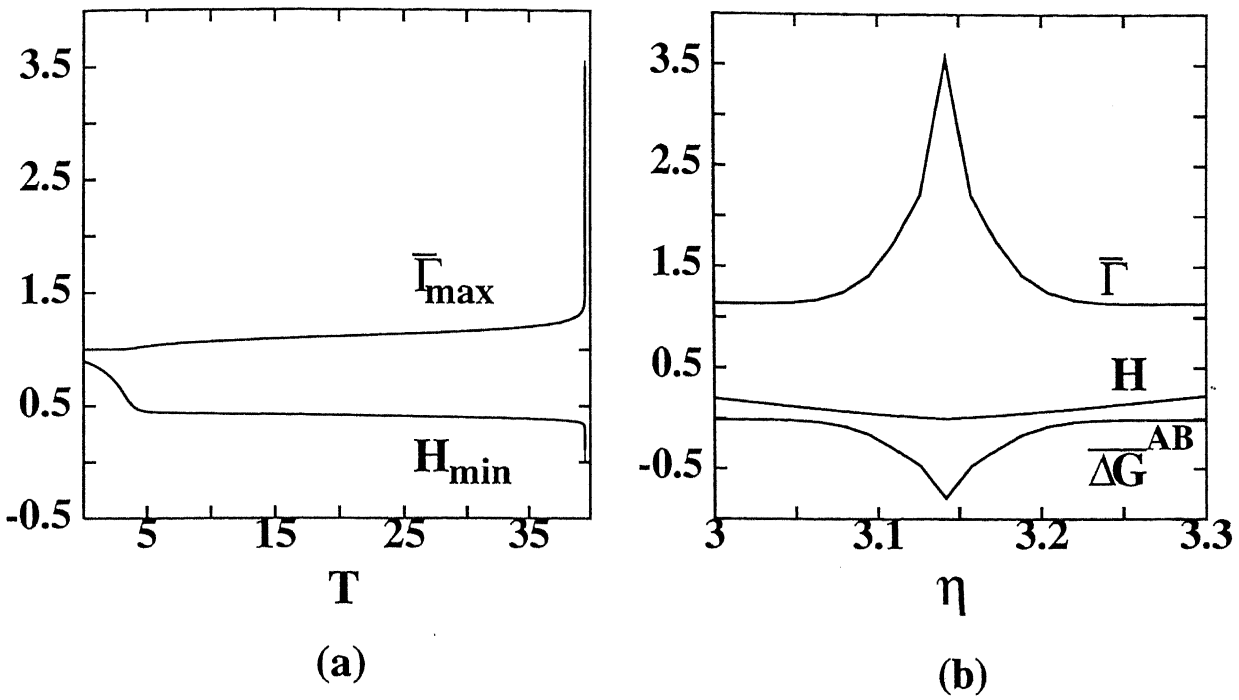

Fig. 3.12 (a) Variation of nondimensional minimum film thickness and maximum receptor concentration with nondimensional time. (b) Nondimensional profiles at the time of rupture around the position where rupture takes place. Both are for polar case, all parameter values being same as in fig.3.6. and bending is the stabilising factor.

entire qualitative behaviour of the system (the polar case). The concentration and surface coverage of the receptors are important in these cases. The model adopted here is found to be adequate to represent the actual physical phenomena and flexible enough to account for different cases with largely varying system parameters. Further works can be done in this respect using different approach to describe the modified interactions. Several other parameter cases can be tested, even with this model. The effect of bending moment, Marangoni effect, variation of the surface diffusion coefficient etc., can be included in these studies. Moreover, this approach can be generalised for the cell-cell interactions.

Bibliography

[1] Buck, C. A., and Horwitz, A. F., J. Cell Science. 8, 231 (1987).

[2] Gieger, B., Volk, T., Volberg, T., and Bendori, R., J. Cell Science. 8, 251 (1987).

[3] Yih, C. S., Phys. Fluids 6, 321 (1963).

[4] Williams, M. B., and Davis, S. H., J. Colloid Interface Sci. 90, 220 (1982).

[5] Gallez, D., and Coakley, W. T., Progr. Biophys. Molec. Biol., 48, 155 (1986).

[6] Sharma, A., and Ruckenstein, E., J. Colloid Interface Sci. 113, 456 (1986).

[7] Gallez, D., Colloids and Surfaces B: Biointerfaces. 2, 273 (1994).

[8] Bell, G. I., Dembo, M., and Bongrand, P., Biophys. J., 45, 1051 (1984).

[9] Singer, S.J., Science, 225 ,1671 (1992).

[10] Evans, E. A., Biophys. J. 14, 921 (1974).

[11] van Oss, C. J., Colloids Surfaces A: 78 (1993).

[12] van Oss, C. J., Chawdhury, M. K., annd Good, R. J., Chem. Rev. 88, 927 (1988).

[13] Canuto, C., Hussaini, M.Y., Quarteroni, A., and Zang, T.A., "Spectral Methods in Fluid Dynamics." Springer-Verlag, New York (1988).

[14] Orszag, S. A., Stud. Appl. Math. 51, 253 (1972).

[15] Hussaini, M. Y., and Zang, T. A., Ann. Rev. Fluid Mech. 19, 339 (1987).

[16] Burelbach, J.P., Bankoff, S.G., and Davis, S. H., J. Fluid Mech. 195,463 (1988).

[17] Sharma, A., and Jameel, A. T., J. Colloid Interface Sci. 161, 190 (1993).

[18] van Oss, C. J., Chawdhury, M. K., annd Good, R. J., Sep Sci. Technl. 24, 15 (1989).

[19] Sharma, A., and Jameel, A. T., J. Colloid Interface Sci. 164, 417 (1993).

[20] Reiter, G., Phys. Rev. Lett. 8, 75 (1992).

[21] Zhao, W., Rafailovich, M. H., Sokolov, J., Fetters, L. J., et al., Phys. Rev. Lett. 70, 1453 (1993).

[22] Cahn, J. W., J. Chem. Phys. 42, 93 (1965).

[23] de Gennes, P. G., Rev. Mod. Phys. 57, 827 (1985).

[24] Grinnel, F., Toda, K. I., and Takadhima , A., J. Cell Science. 8, 199 (1987).